

AD 745906

RRA-T7201
14 July 1972

RRA RADIATION RESEARCH ASSOCIATES
Fort Worth, Texas

INITIAL RADIATION EXPOSURE FROM NUCLEAR WEAPONS

by
R.L. French and L.G. Mooney

Reproduced by
NATIONAL TECHNICAL
INFORMATION SERVICE
U.S. Department of Commerce
Springfield, VA 22151

Interim Report
Contract No. DAHC20-72-C-0123
OCD Work Unit 1118B
for
OFFICE OF CIVIL DEFENSE

DDC
RECEIVED
JUL 27 1972
REGISTERED
B

Approved for public release; distribution unlimited

87

DOCUMENT CONTROL DATA - R & D

(Security classification of title, body of abstract and indexing annotation must be entered when the overall report is classified)

1. ORIGINATING ACTIVITY (Corporate author)		2a. REPORT SECURITY CLASSIFICATION	
RADIATION RESEARCH ASSOCIATES, INC.		UNCLASSIFIED	
		2b. GROUP	
3. REPORT TITLE			
INITIAL RADIATION EXPOSURE FROM NUCLEAR WEAPONS			
4. DESCRIPTIVE NOTES (Type of report and inclusive dates)			
INTERIM REPORT			
5. AUTHOR(S) (First name, middle initial, last name)			
ROBERT L. FRENCH and L. GLENN MOONEY			
6. REPORT DATE	7a. TOTAL NO. OF PAGES	7b. NO. OF REFS	
14 JULY 1972	87	16	
8a. CONTRACT OR GRANT NO.	8b. ORIGINATOR'S REPORT NUMBER(S)		
DAHC20-72-C-0123	RRA T7201		
a. PROJECT NO.	9b. OTHER REPORT NO(S) (Any other numbers that may be assigned this report)		
OCD Work Unit 1118B			
c.			
d.			
10. DISTRIBUTION STATEMENT			
Approved for public release; distribution unlimited.			
11. SUPPLEMENTARY NOTES		12. SPONSORING MILITARY ACTIVITY	
		Office of Civil Defense Office of Secretary of the Army Washington, D. C. 20310	
13. ABSTRACT			
<p>Recent data and methods for predicting the initial radiation exposure at or near the ground surface resulting from the detonation of nuclear weapons were reviewed and evaluated. State-of-the-art methods were then selected or developed for neutron dose, secondary gamma-ray dose from neutron interactions in the air and ground, and fission-product gamma-ray dose occurring during the first minute following a detonation. The neutron and secondary gamma-ray method is based on Straker's discrete ordinates calculations of neutron transport in an air-over-ground geometry and French's first-last collision method for source height effects. The fission-product gamma-ray model is based on Monte Carlo air transport calculations by Marshall and Wells and incorporates source spectra, source decay rates, cloud rise approximations, and hydrodynamic enhancement treatments based on the work of a number of previous investigators. The methods and the incorporated data were validated through extensive comparison with weapon test results and with other calculated and semi-empirical data. From these comparisons, it was concluded that neutron doses may be predicted within approximately 25% and that the total gamma-ray exposures may be predicted within approximately 50% if the weapon characteristics and the burst conditions are known. For convenience in predicting initial radiation exposures, highly simplified models were derived from the results of extensive parametric calculations performed with the detailed methods.</p>			

14. KEY WORDS	LINK A		LINK B		LINK C	
	ROLE	WT	ROLE	WT	ROLE	WT
Air transport Fission product gamma rays Initial radiation neutrons radiation environment secondary gamma rays simplified models weapons radiation						

RRA-T7201
15 July 1972

INITIAL RADIATION EXPOSURE FROM NUCLEAR WEAPONS

by

R. L. French and L. G. Mooney

Office of Civil Defense
Office of the Secretary of the Army
Washington, D. C. 20310

OCD Review Notice

This report has been reviewed in the Office of Civil Defense and approved for publication. Approval does not signify that the contents necessarily reflect the views and policies of the Office of Civil Defense

Interim Report

Contract No. DAHC20-72-C-0123
OCD Work Unit 1118B

Radiation Research Associates, Inc.
3550 Hulen Street
Fort Worth, Texas 76107

Approved for public release: distribution unlimited

TABLE OF CONTENTS

	<u>Page</u>
ABSTRACT	ii
LIST OF FIGURES	iv
LIST OF TABLES	vi
SUMMARY	vii
I. INTRODUCTION	1
II. INITIAL RADIATION SOURCES	4
2.1 Neutrons	5
2.2 Secondary Gamma Rays	8
2.3 Fission-Product Gamma Rays	9
III. METHODS DESCRIPTION	11
3.1 Neutrons	13
3.2 Secondary Gamma Rays	23
3.3 Fission-Product Gamma Rays	29
IV. METHODS EVALUATION	38
4.1 Neutrons	40
4.2 Secondary Gamma Rays	51
4.3 Fission-Product Gamma Rays	53
V. SIMPLIFIED MODEL	67
5.1 Charts	67
5.2 Equation	69
VI. CONCLUSIONS	76
REFERENCES	77
APPENDIX	79

LIST OF FIGURES

<u>Figure</u>		<u>Page</u>
1.	Relative Neutron Dose vs Slant Range for Different Types of Neutron Sources	17
2.	Fast-Neutron Energy Spectra at a Range of 900 Meters in Air	18
3.	First and Last Collision Fractions	22
4.	Percentage of Secondary-Gamma Dose vs Slant Range from 14-MeV Neutron Source from Various Reactions in Air and Ground	24
5.	Percentage of Secondary-Gamma Dose vs Slant Range from BREN Source from Various Reactions in Air and Ground	25
6.	Secondary-Gamma Dose vs Slant Range for Fission and 14-MeV Neutron Sources	26
7.	Secondary-Gamma Dose vs Slant Range for Several Devices	28
8.	Effect of Cloud Rise and Hydrodynamic Enhancement on Fission-Product Gamma Dose vs Slant Range from Nominal 1-KT Device	37
9.	Neutron Activation Fluences and Dose vs Slant Range for Device No. 6	41
10.	Neutron Activation Fluences and Dose vs Slant Range for Device No. 10	42
11.	Neutron Activation Fluences and Dose vs Slant Range for Device No. 11	43
12.	Neutron Activation Fluences and Dose vs Slant Range for Device No. 12	44
13.	Neutron Activation Fluences and Dose vs Slant Range for Device No. 13	45

<u>Figure</u>	<u>Page</u>
14. Neutron Activation Fluences and Dose vs Slant Range for Device No. 14	46
15. Neutron Activation Fluences and Dose vs Slant Range for Device No. 18	47
16. Neutron Dose and Thermal Neutron Fluence vs Slant Range for BREN Source at Height of 8 Meters	49
17. Neutron Dose vs Slant Range for HENRE Source	50
18. Secondary-Gamma Dose vs Slant Range for HENRE Source	52
19. Calculated and Measured Gamma-Ray Dose vs Slant Range for Device No. 6	54
20. Calculated and Measured Gamma-Ray Dose vs Slant Range for Device No. 10	55
21. Calculated and Measured Gamma-Ray Dose vs Slant Range for Device No. 11	56
22. Calculated and Measured Gamma-Ray Dose vs Slant Range for Device No. 12	57
23. Calculated and Measured Gamma-Ray Dose vs Slant Range for Device No. 13	58
24. Calculated and Measured Gamma-Ray Dose vs Slant Range for Device No. 14	59
25. Calculated and Measured Gamma-Ray Dose vs Slant Range for Device No. 18	60
26. Calculated and Measured Gamma-Ray Dose vs Slant Range for Device No. 19	62
27. Calculated and Measured Gamma-Ray Dose vs Slant Range for Device No. 21	63
28. Calculated and Measured Gamma-Ray Dose vs Slant Range for Device No. 23	64
29. Calculated and Measured Gamma-Ray Dose vs Slant Range for Device No. 25	65

LIST OF TABLES

<u>Table</u>		<u>Page</u>
I.	Neutron Leakage Spectra of Representative Nuclear Weapons	7
II.	Gamma-Ray Spectra from Decay of ^{235}U Fission Products	10
III.	$4\pi\text{R}^2$ Neutron and Secondary Gamma-Ray Dose From Point Isotropic Neutron Source in Air-over-Ground Geometry	16
IV.	$4\pi\text{R}^2$ Dose from Point Isotropic Gamma-Ray Source in Infinite Air	31
V.	Test Devices Selected for Comparison of Calculated and Measured Neutron and Gamma-Ray Dose	39

SUMMARY

There has been increasing recognition that initial radiation may often be the controlling effect when civilian populations are exposed to the detonation of a nuclear weapon. Concurrent improvements in radiation transport calculations and in techniques for taking into account the many factors that influence the initial radiation exposure from nuclear weapons have led to the development of consistent and relatively accurate methods for predicting initial radiation exposures. This report reviews these developments and presents state-of-the-art data and techniques for defining the free-field initial radiation environment produced at or near the ground surface by a wide variety of weapon types, yields and burst conditions.

The initial radiation environment is defined in terms of the free-field dose or exposure from neutrons, secondary gamma-rays produced by neutron interactions with the constituents of the air and ground, and gamma-rays emitted from the decay of fission products during the first minute following the detonation. In addition to a definition of the radiation sources, the problem of calculating the initial radiation environment from a nuclear weapon requires a mathematical method for performing transport calculations in an air-over-ground geometry, and an appropriate set of cross section data. In the case of fission-product gamma-rays, air density distributions as a function of time are also required to account for the hydrodynamic effect.

Transport calculations are rarely performed directly for specific cases. Detailed discrete ordinates neutron transport calculations have been performed by Straker for several source neutron energies and a limited number of source and detector heights. The neutron method given here weights Straker's results by the number of neutrons escaping the source at (or in the vicinity of) each of the individual source energies.

considered in the calculations. The results (i.e., dose versus distance) from all source energies are then combined and adjusted to the desired source and detector height using French's first-last collision method. Secondary gammas from neutron interactions in the air and ground are treated as an extension of the neutron problem.

Fission-product gamma rays contribute the largest fraction of the initial gamma-ray dose in many cases of interest, and are the most tedious of all initial radiation components to calculate. The fission-product gamma-ray source expands from essentially a point source to a volume source over the time span of interest (the first minute). At the same time, it moves upward, decreases in intensity, and undergoes changes in energy spectrum. Finally, the fission-product gamma transport in air is strongly influenced by the perturbation of the air by the blast (hydrodynamic effect). The fission-product gamma-ray model reported here is based on Monte Carlo air transport calculations by Marshall and Wells and incorporates source spectra, source decay rates, cloud rise approximations, and hydrodynamic enhancement treatments based on the work of a number of previous investigators.

Extensive comparisons between calculations performed with these detailed methods and the results of weapons test indicate that methods predict initial radiation exposures generally within 25 to 50%. However, the detailed methods are not well suited for routine practical application because they require the use of machine codes and a thorough understanding of the input data and of the many steps involved. Therefore a highly simplified model based on the analysis of extensive calculations performed with the detailed method was developed. This model, which requires the use of only six charts and one equation, gives results that agree with the detailed calculations within 20% in most cases and within 45% in virtually all cases.

I. INTRODUCTION

During the past decade there has been increasing recognition that initial radiation may often be the controlling effect when civilian populations are exposed to the detonation of a nuclear weapon. This recognition results from a better understanding of initial radiation production and propagation coupled with a trend toward moderate yield weapons delivered by multiple reentry vehicles. These smaller weapons invariably produce higher initial radiation exposures relative to blast, thermal and other effects than do the multi-megaton weapons once considered to be the principal threat to civilian populations.

Recent improvements in radiation transport calculations^{1,2} and in technique^{3,5} for taking into account the many factors that influence the initial radiation exposure from nuclear weapons have led to the development of consistent and relatively accurate models for predicting initial radiation exposures.^{5,6} The purpose of this report is to review these developments and to present state-of-the-art data and techniques for defining the free-field initial radiation environment produced at or near ground surface by a wide variety of weapon types, yields and burst conditions.

The initial radiation environment is defined here in terms of the free-field dose or exposure from neutrons, secondary gamma rays produced by neutron interactions with the constituents of the air and ground, and fission-product gamma rays emitted during the first minute following the detonation. Evaluation of the energy and angle distributions required for the evaluation of transient radiation effects is beyond the scope of the report.

The significant sources of initial radiation are described in Section II. These include prompt neutrons (i.e., those emitted simultaneously with the fission or fusion events), gamma rays from the decay of fission products, and secondary gamma rays from neutron interactions (capture or inelastic scattering) with the nuclei of the air and ground. Sources of lesser importance are delayed neutrons, secondary gamma rays from neutron interactions with the materials of the device, and prompt fission gamma rays (emitted simultaneously with fission). Except for certain special weapon designs or applications, these latter gamma-ray components may normally be neglected in predicting the total doses or exposures because they are almost entirely absorbed by the dense weapon materials before the weapon has blown completely apart.^{7,8}

In addition to a definition of the radiation sources, the problem of calculating the initial radiation environment from a nuclear weapon requires a mathematical method for performing transport calculations in an air-over-ground geometry, and an appropriate set of cross section data. In the case of fission-product gamma rays, air density distributions as a function of time are also required to account for the hydrodynamic effect.

Transport calculations are rarely performed directly for specific cases. The complicated and time-consuming neutron transport calculations are usually performed for several source neutron energies and only a severely limited number of source and detector heights. The results of such calculations may be weighted by the number of neutrons escaping the source at (or in the vicinity of) each of the individual source energies considered in the calculations. The results (i.e., dose versus distance, or other desired quantities) from all source energies may then be combined and adjusted in some way to take into account the air density and the source and detector heights.

Secondary gammas from neutron interactions in the air and ground may

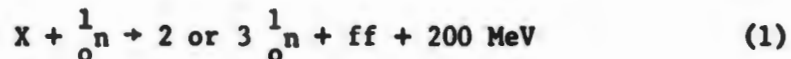
be treated as an extension of the neutron problem, but in this case, the ground composition may become an important parameter. In particular, the hydrogen content of the ground has a strong influence on the intensity and spatial distribution of thermal neutrons (hence, secondary gamma production) at the interface.

Fission-product gamma rays contribute the largest fraction of the initial gamma-ray dose in many cases of interest, and are the most tedious of all initial radiation components to calculate. The fission-product gamma-ray source expands from essentially a point source to a volume source over the time span of interest (the first minute). At the same time, it moves upward, decreases in intensity, and undergoes changes in energy spectrum. Finally, the fission-product gamma transport in air is strongly influenced by the perturbation of the air by the blast (hydrodynamic effect). Because of these complicating factors, most fission-product gamma-ray dose predictions were, until recently, made using semi-empirical methods which left something to be desired in terms of accuracy and broad applicability.

Section III describes data and detailed procedures for calculating each of the major initial radiation components. Extensive comparisons given in Section IV indicate that these methods predict initial radiation exposures generally within 25 to 50%. However, the detailed methods are not well suited for routine practical application because they require the use of machine codes and a thorough understanding of the input data and of the many steps involved. Therefore a highly simplified model based on the analysis of extensive calculations performed with the detailed method was developed as part of the present study. This model is given in Section V.

2.1 Neutrons

Fission neutrons are produced by the reaction



where 1_0n is the symbol for neutrons, ff denotes fission fragments, and X represents either of the isotopes ${}^{233}_{92}\text{U}$, ${}^{235}_{92}\text{U}$, or ${}^{239}_{94}\text{Pu}$. These isotopes are fissionable by neutrons of any energy and thus will sustain a chain reaction. They are also reasonably stable so that they can be stored without appreciable decay. The isotopes ${}^{238}_{92}\text{U}$ and ${}^{232}_{90}\text{Th}$ will suffer fission by neutrons of high energy only and cannot sustain a chain reaction. All of these reactions produce essentially the same characteristic neutron fission spectrum.

Four thermonuclear fusion reactions are of interest for the production of energy.



where ${}^1_1\text{H}$, ${}^2_1\text{D}$ and ${}^3_1\text{T}$ are isotopes of hydrogen (hydrogen, deuterium and tritium) and ${}^4_2\text{He}$ is an isotope of helium. Reactions (2) and (3) occur with equal probability. A high percentage of the neutrons produced by Reaction (4) have energies of approximately 14 MeV.

The number of leakage neutrons (i.e., neutrons that actually escape from the weapon as it detonates) and their distribution in energy are required to properly define the neutron source. Although the neutron leakage may be anisotropic in some cases, it is usually necessary to treat the neutrons as though they are emitted from a point isotropic source.

The neutron source term can be precisely defined only by taking into account the design of the specific weapon being considered. The important parameters are the fission-to-fusion ratio, and the amount and configuration of the fuel, high explosive, tamper, and case materials. Detailed source term calculations cannot be discussed here. However, rough approximations of neutron source terms can be made for "nominal" weapons without detailed calculations which consider all of these parameters.

Table I gives representative neutron source terms for three different types of weapons. The "fission" weapon is representative of relatively low-leakage pure fission weapons. The "thermonuclear" weapon is similar to the typical intermediate-yield TN weapon described in Reference 9.* The "intermediate" weapon may be considered representative of a relatively high-leakage fission weapon or a low-yield thermonuclear weapon with a very high fission fraction.

*See appendix for a comparison of the radiation exposures produced by the two thermonuclear weapons.

Table I. Neutron Leakage Spectra of Representative Nuclear Weapons

Energy Interval (MeV)	(neutrons/KT)		
	Weapon Type		
	Fission	Intermediate	Thermonuclear
12.2 - 15.0	-	5.08+20	1.62+22
10.0 - 12.2	-	1.81+20	8.53+21
8.18 - 10.0	7.32+20*	3.82+20	6.08+21
6.36 - 8.18	1.27+21	1.86+21	5.46+21
4.06 - 6.36	3.00+21	1.02+22	6.41+21
2.35 - 4.06	8.90+21	2.66+22	1.22+22
1.11 - 2.35	2.52+22	5.99+22	2.84+22
0.111 - 1.11	2.84+22	8.47+22	6.18+22
0.0033 - 0.111	2.22+22	5.37+21	1.71+23
Total	9.97+22	1+90+23	3.16+23

*Read 7.32+20 as 7.32×10^{20}

2.2 Secondary Gamma Rays

Potentially important sources of secondary gamma rays result from the inelastic scattering of high-energy neutrons by the nuclei of the air and ground, and the capture of thermal neutrons by the nitrogen-14 in the air and by various elements in the ground. The relative importance of the inelastic and capture gamma rays depends strongly upon the neutron spectrum of the source.

Any determination of the intensity of inelastic and capture gamma rays must rely primarily upon analysis because of the difficulty in distinguishing the source of the different gamma rays measured in field tests. The first step in the analysis is that of neutron transport calculations. The local source strength of inelastic gamma rays is an energy dependent response to the local fluence of neutrons. Once the source intensity due to interactions in air and ground is known, a gamma ray transport calculation must be performed to obtain the intensity at detectors of interest. These steps may be performed separately or, as is the case in recent work, they may be combined into a single analysis program.

The original source for all secondary gamma rays produced in the air and ground is the neutrons produced by the detonation of the weapon, therefore the neutron source discussion and the representative source spectra given in Section 2.1 are applicable to secondary gamma rays.

2.3 Fission-Product Gamma Rays

Gamma rays produced by the decay of fission products following a fission detonation are one of the principal sources of radiation in the initial radiation time regime (the first one or two minutes following the detonation). The intensity of fission-product gamma rays reaching a location of interest is affected by the complex source and media dynamics consisting of the formation and evolution of the fireball, the cloud expansion and rise, and the decay of the fission products with time. The fission products disperse throughout the cloud with the passage of time and the shape of the cloud may vary from spherical to toroidal as the materials forming the cloud rise through the atmosphere. The formation of the fireball and the expansion and rise of the cloud depends upon weapon yield, weapon design, atmospheric conditions, and other parameters.

Table II lists fission-product gamma ray spectra as a function of time following ^{235}U fission as measured by Engle and Fisher.¹⁰ The gamma-ray yields and energy spectra from the fission products of ^{233}U and ^{239}Pu are similar enough to those of ^{235}U that the latter may be used as a reasonable approximation for most purposes.

Table II. Gamma-Ray Spectra from Decay
of ^{235}U Fission Products

(photons·fission⁻¹·sec⁻¹·MeV⁻¹)

Energy Interval Midpoint (MeV)	Time Interval (sec)				
	0.2-0.5	1.0-2.0	4.0-5.5	10-13	35-45
0.175	1.33 +0*	5.37 -1	3.20 -1	1.45 -1	3.85 -2
0.261	6.87 -1	3.37 -1	1.95 -1	9.30 -2	2.48 -2
0.369	4.60 -1	2.35 -1	1.31 -1	6.17 -2	1.86 -2
0.502	4.92 -1	2.98 -1	1.65 -1	7.19 -2	1.67 -2
0.662	3.28 -1	1.94 -1	1.03 -1	4.66 -2	1.19 -2
0.852	3.00 -1	1.53 -1	6.50 -2	3.10 -2	1.03 -2
1.075	2.18 -1	1.33 -1	5.62 -2	2.55 -2	7.91 -3
1.337	1.45 -1	7.72 -2	3.73 -2	1.95 -2	6.84 -3
1.643	8.68 -2	5.06 -2	2.66 -2	1.20 -2	4.06 -3
1.998	6.17 -2	3.46 -2	1.69 -2	7.56 -3	2.47 -3
2.405	3.86 -2	2.17 -2	1.09 -2	5.12 -3	1.78 -3
2.865	2.87 -2	1.62 -2	7.12 -3	3.51 -3	1.26 -3
3.383	1.85 -2	1.07 -2	5.29 -3	2.19 -3	6.10 -4
3.956	9.71 -3	5.74 -3	2.64 -3	1.24 -3	4.60 -4
4.587	7.96 -3	3.37 -3	1.55 -3	7.12 -4	2.12 -4
5.277	1.67 -3	1.21 -3	5.86 -4	2.94 -4	8.95 -5
6.028	1.94 -3	7.20 -4	4.54 -4	1.65 -4	4.16 -5

*Read 1.33+0 as 1.33×10^0

III. METHODS DESCRIPTION

Transport calculations for initial radiation are not basically different from transport calculations for any other type of radiation. However, on the macroscopic level, there are several effects peculiar to initial radiation transport.

One is the hydrodynamic effect, the term applied to the perturbation of the air by the energy imparted by the blast. This effect has a strong influence on the propagation of fission-product gamma rays through the air since most of them are emitted while the shock front moves through the air generating compressed and rarified layers. A further complication in calculating the transport of fission-product gamma rays is the consideration of the time-dependent parameters of cloud rise and source decay.

As compared to most transport problems, there are considerable differences in the geometry and composition of the media involved in initial radiation transport. Normally, the detonation and most of the radiation propagation occurs in air, a very low density material. The air is bounded on one side by the ground which is approximately one thousand times as dense. The air-ground interface, consequently, has a profound influence on the radiation transport.

The presence of an air-ground interface can increase or decrease initial radiation intensities as much as an order of magnitude as compared to intensities at corresponding distances in an infinite air medium. The direction and magnitude of the interface effect depends upon the type of radiation, the proximity of the ground, and the source-detector separation distance.

At source-detector separation distances less than a mean-free-path in air, localized reflection from the ground generally tends to increase

the intensity of fast neutrons and fission-product gamma rays. However, the initial radiation environments are normally not of interest at such short distances because of the dominance of other weapon effects. At larger distances, these components tend to decrease as either the source or the detector approaches the ground. As a limiting case, the fast-neutron intensity, as compared to infinite air, may be reduced by a factor of 5 or more when both the source and detector are at the ground surface. Although the trends are the same, the interface effects on fission-product gamma rays are not quite as strong as is the case for fast neutrons.

The reduction in radiation intensities at large distances described above may be explained by the fact that the ground acts as a better absorber of radiation than does the air that it displaces. The effect of the interface on thermal neutrons and on secondary gamma-ray production is much more complicated because of two factors; (1) the ground is a better thermalizer of neutrons than is the air, and (2) the ground composition has a significant influence on both thermalization and on secondary gamma-ray production.

Because of the impracticality of treating air-ground interface effects for all combinations of source and detector heights in the basic transport calculations, it is common practice to use the height conditions for which data are available and are closest to those desired and, where possible, make some adjustment to account for the difference between the desired heights and those actually used.

The methods which are described below are concerned with the practical application of the results of radiation transport calculations; detailed descriptions of radiation transport methods are beyond the scope of the report. The methods were selected by the authors as being representative of the state-of-the-art and well-suited for the development of simplified models such as the one described in Section V. Readers interested in the relationship of those methods to others, or in the basic transport calculations, are referred to the cited source documents which give a somewhat broader treatment.

3.1 Neutrons

Straker's calculations of neutron transport data for an air-over-ground geometry¹ provide a basis for techniques to predict the neutron radiation environment produced by the detonation of nuclear weapons. This section summarizes the transport data, describes the application techniques, and compares the results with measurements.

It is generally not feasible to calculate the neutron environment produced by a given detonation by starting from first principles and considering the fundamental phenomenology of all the pertinent physical processes. Alternatively, the overall problem is divided into three parts: 1) neutron source definition, 2) neutron transport in air, and 3) special adjustments. These parts may be treated more or less independently.

The number of leakage neutrons (i.e., neutrons that actually escape from the weapon as it detonates) and their distribution in energy are required to properly define the neutron source. Although the neutron leakage may be anisotropic in some cases, it is usually necessary to treat the neutrons as though they are emitted from a point isotropic source. Some of the other considerations in defining neutron sources were discussed in Section 2.1.

Neutron Transport Data

Straker's air-over-ground neutron transport calculations¹ performed with the DOT discrete ordinates code¹¹ give the spatial, energy, and angle distributions of neutrons and secondary gamma rays at the air-ground interface. The secondary gamma rays, which will be discussed in more detail in Section 3.2, are from inelastic scattering of fast neutrons and capture of both fast and thermal neutrons in the air and ground. The neutrons are emitted from a point isotropic source located 15 meters above the ground. An air density of 1.1×10^{-3} gm/cm³ was assumed for the calculations. ENDF/B cross sections were used.

Separate results are given for each of nine source neutron groups or bands:

<u>No.</u>	<u>Energy (MeV)</u>
1	12.2 - 15.0
2	10.0 - 12.2
3	8.18 - 10.0
4	6.36 - 8.18
5	4.06 - 6.36
6	2.35 - 4.06
7	1.108 - 2.35
8	0.111 - 1.108
9	0.0033 - 0.111

The distribution of neutrons in each source group is uniform except the 0.0033 - 0.111 MeV group which has a 1/E distribution.

The neutron and gamma-ray dose ($4\pi R^2$ cm² rad per source neutron) is given at ranges (R) of 40, 79, 153, 240, 300, 390, 600, 900, 1200, and 1500 meters. Also given is the neutron fluence in each of 22 energy groups between 0 and 15 MeV. In a subsequent study,⁶ these results were extrapolated for additional ranges of 2000, 2500, and 3500 meters, and some of the very short ranges were deleted because they are of little interest in weapons applications. The extrapolations to larger ranges were guided by the results of limited additional calculations for larger ranges performed

by Straker for the 12.2 - 15.0 MeV source and for a fission neutron source⁴.

The complete set of data extracted from Straker's calculations include the fluence in each of 15 energy groups and are tabulated in Reference 6. The neutron and secondary gamma-ray dose data required by the methods described in this report are given in Table III. These data are Henderson single-collision tissue dose given in Reference 17.

The dependence of Straker's neutron transport data upon source energy is illustrated by Figure 1, which shows the neutron dose as the fraction of the dose at the source (D/D_0) versus distance for three different types of neutron sources each at a height of 15 meters. The dose from the 12.2 - 15.0 MeV source (which is representative of the 14-MeV neutrons from a fusion source) decreases least rapidly with increasing range. The representative thermonuclear weapon source⁹ has a high percentage of fusion neutrons, but the D/D_0 curve decreases with distance more like that for the pure fission source. The fission source is an idealized source and does not include spectral modification by the weapon materials.

Figure 2 compares the energy spectra at a range of 900 meters resulting from the same fission, thermonuclear, and 14-MeV neutron sources. At this range, virtually all of the neutrons have undergone scattering in the air and/or ground. Nonetheless, it is seen that there are still distinct differences among the various spectra.

It is apparent from the above comparisons of results calculated with Straker's data that both the neutron spectrum and the number of neutrons from a specific weapon must be taken into account in order to accurately predict the neutron environment at a given location. Some degree of success has been achieved in using representative spectra for

Table III. $4\pi R^2$ Neutron and Secondary Gamma-Ray Dose From Point Isotropic Neutron Source in Air-Over-Ground Geometry

Source Energy (MeV)	$(\text{cm}^2 \text{ rad/source neutron})$								
	153.1	300.3	600.2	900.1	1200	1500	2000	2500	3500
	R, Slant Range (meters)								
0.0033 - 0.111	2.610-10*	2.789-11	5.259-14	3.919-17	2.289-20	6.979-24	9.629-30	1.329-35	0.000+00
0.111 - 1.11	2.130-09	1.059-09	1.460-10	1.639-11	1.709-12	1.629-13	3.239-15	6.439-17	2.549-20
1.11 - 2.35	3.789-09	2.329-09	5.919-10	1.160-10	1.869-11	3.059-12	1.489-13	7.329-15	1.749-17
2.35 - 4.06	4.230-09	2.880-09	1.009-09	2.809-10	6.899-11	1.679-11	1.589-12	1.509-13	1.359-15
4.06 - 6.36	4.730-09	3.130-09	1.140-09	3.550-10	9.799-11	2.619-11	2.899-12	3.219-13	3.969-15
6.36 - 8.18	4.989-09	3.480-09	1.440-09	5.030-10	1.559-10	4.569-11	5.899-12	7.629-13	1.269-14
8.18 - 10.0	4.930-09	3.470-09	1.390-09	4.840-10	1.479-10	4.500-11	6.179-12	8.500-13	1.599-14
10.0 - 12.2	4.880-09	3.349-09	1.250-09	4.140-10	1.240-10	3.509-11	4.279-12	5.220-13	7.779-15
12.2 - 15.0	4.930-09	3.250-09	1.170-09	3.679-10	1.050-10	2.949-11	3.549-12	4.280-13	6.219-15
	Neutron Dose**								
0.0033 - 0.111	4.899-10	1.830-10	4.239-11	1.629-11	6.559-12	2.749-12	6.449-13	1.509-13	8.350-15
0.111 - 1.11	4.930-10	3.230-10	7.719-11	2.059-11	7.179-12	2.869-12	6.219-13	1.349-13	6.349-15
1.11 - 2.35	3.990-10	3.550-10	1.300-10	3.579-11	1.039-11	3.429-12	5.399-13	8.499-14	2.099-15
2.35 - 4.06	2.849-10	2.700-10	1.309-10	4.619-11	1.449-11	4.569-12	6.670-13	9.729-14	2.070-15
4.06 - 6.36	2.490-10	2.290-10	1.150-10	4.460-11	1.529-11	5.119-12	8.250-13	1.329-13	3.460-15
6.36 - 8.18	4.550-10	4.180-10	2.250-10	5.889-11	3.829-11	1.469-11	2.969-12	6.039-13	2.480-14
8.18 - 10.0	6.670-10	6.159-10	3.340-10	1.479-10	5.909-11	2.349-11	5.049-12	1.079-12	5.019-14
10.0 - 12.2	9.030-10	8.270-10	4.230-10	1.820-10	7.239-11	2.879-11	6.189-12	1.329-12	6.169-14
12.2 - 15.0	9.420-10	8.550-10	4.300-10	1.850-10	7.219-11	2.969-11	6.749-12	1.529-12	7.949-14
	Secondary Gamma Dose**								

*Read 2.610-10 as 2.610×10^{-10}

**Henderson single collision tissue dose (Ref. 17)

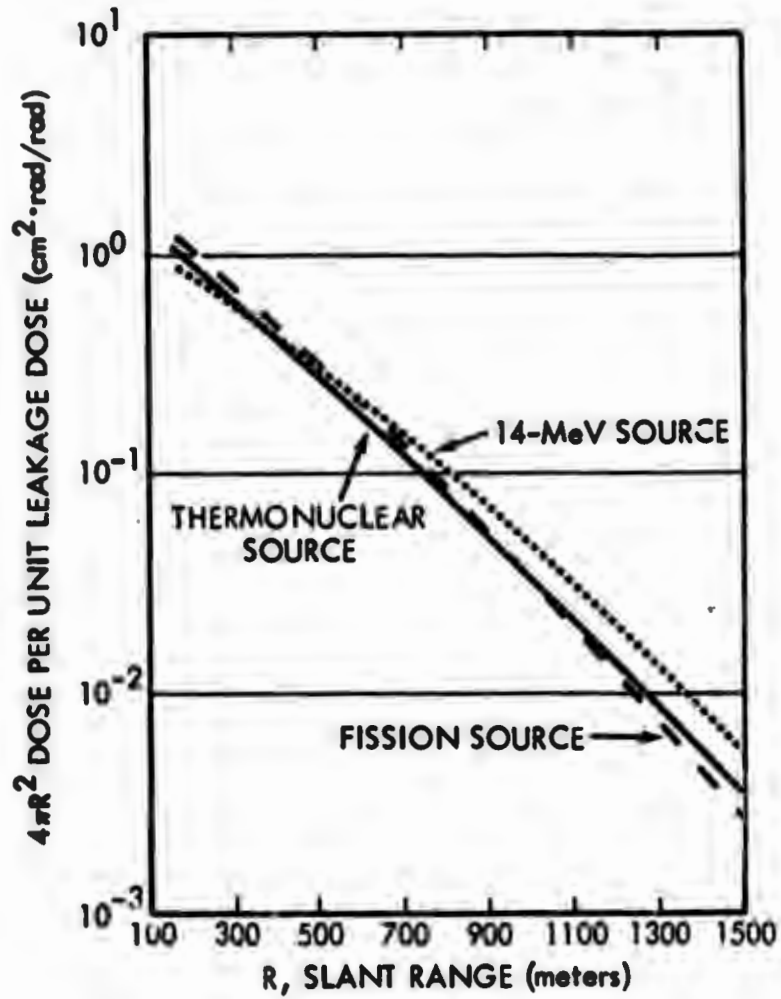


Figure 1. Relative Neutron Dose vs Slant Range for Different Types of Neutron Sources

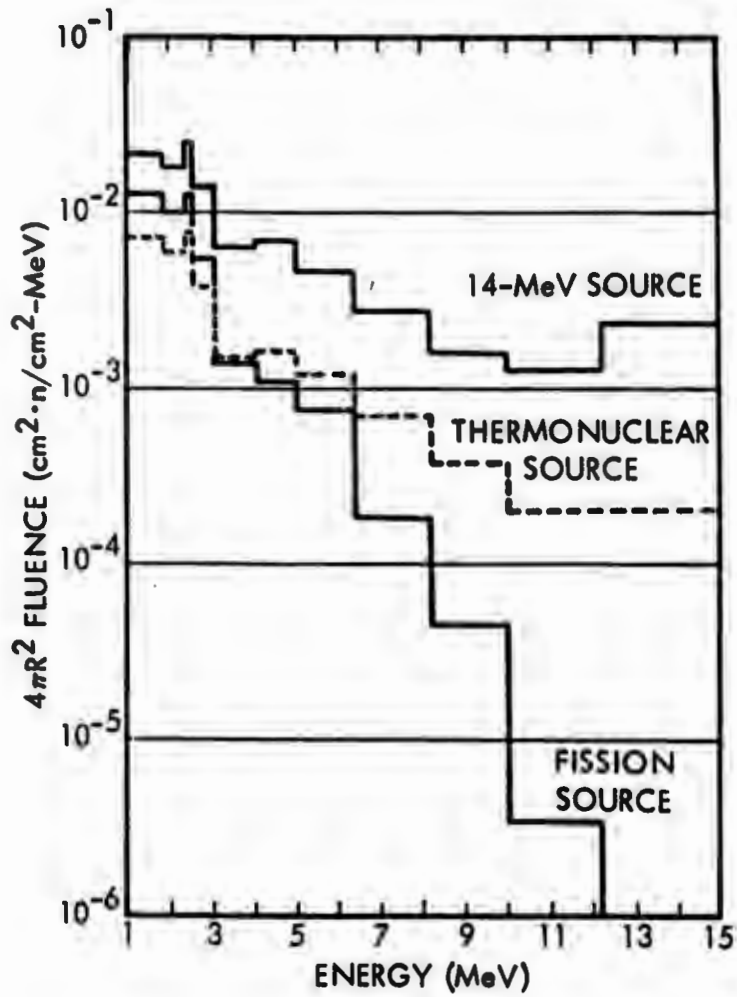


Figure 2. Fast-Neutron Energy Spectra at a Range of 900 Meters in Air

different "categories" of weapons as indicated in Section 2.1, but there may be considerable differences within a given category, particularly in the number of leakage neutrons.

Source Strength

The first step required to predict the neutron exposure from a given nuclear weapon consists of integrating the weapon's neutron leakage spectrum over energy intervals corresponding to the 9 source energy bands listed in Table III. Normally, the neutron source strength is specified in terms of the number of leakage neutrons per KT (or the number of neutrons/MeV per KT) in each of a number of energy groups. The source term processing in this case involves the use of a known, or assumed, distribution within the original energy groups in order to regroup to the desired 9 source energy bands. Source terms for representative weapons are described in Section 2.1.

The next step consists of multiplying the neutron exposure as a function of range, $D(R)_{En}$, for each source energy band, En , by the number of leakage neutrons, S_{En} , for the corresponding source energy band

$$D(R) = \sum_{n=1}^{n=9} S_{En} D(R)_{En} \quad (6)$$

Since $D(R)_{En}$ from Table III is in the form of $4\pi R^2$ rad per source neutron, $D(R)$ has units of $4\pi \text{cm}^2$ rad. The absolute neutron dose is given by

$$D_n(R) = \frac{D(R)}{4\pi R^2} \quad (7)$$

$D(R)$ as computed from the Table III data is for an air density of $1.1 \times 10^{-3} \text{ gm/cm}^3$ and a source height of 15 meters. If the neutron dose,

$D_n(R)$, is to be calculated for a different air density, $D(R)$ must be interpolated for a scaled value of range, R' . The scaled range is given by

$$R' = \frac{\rho R}{1.1 \times 10^{-3}} = 900.91 \rho R \quad (8)$$

where ρ is the new air density and R is the original range in air of density ρ at which the neutron dose is required. Note that the original range R is still used in the denominator of Equation 7; R' is used only for obtaining values of $D(R)$.

Air-Ground Interface Effect

A variation of the first-last collision method³ may be used to adjust neutron transport data to source heights other than those for which the basic calculations were originally performed. This method was originally developed for the purpose of adding interface perturbations to infinite air results, but subsequent study has shown that it is quite effective for simply adjusting from one height to another.

The first-last collision method provides an estimate of the interface effect by considering 1) the influence of the ground beneath the source upon the number of first collisions in air in the vicinity of the source and 2) the influence of the ground beneath the detector upon the number of last collisions which occur in air in the vicinity of the detector. Scattering of neutrons from the ground is treated at both the source and the detector by an albedo approach. The first-last collision method applies only to the scattered component and may be expected to be valid only when the source-detector separation distance is sufficiently large for multiple scattering to be dominant.

The first-last collision method gives a source height factor, $f(H'_S)$,

and a detector height factor, $f(H_D)$, which may be applied to the fluence or the dose $I(R)$ in an infinite air medium to obtain the fluence or dose at the same separation distance (R) but where the source is at height H_S and the detector is at height H_D above the ground:

$$I(H_S, H_D, R) = f(H_S) f(H_D) I(R). \quad (9)$$

The source height factor $f(H_S)$ is the effective fraction of the source leakage neutrons which undergo first collisions in air; hence, it affects equally the multiple scattered neutrons arriving from all directions at a distant detector. It is called an effective fraction because it includes uncollided neutrons which strike the ground but are scattered back out to undergo "first" collisions in air. Similarly, $f(H_D)$ is the fraction (as compared to infinite air) of neutrons which undergo their last collision in air and it includes an adjustment for reflection from the ground in the vicinity of the detector.

If $I(H_S, H_D, R)$ is already known from a transport calculation performed explicitly for H_S , H_D , and R , the intensity at the same detector height, H_D and range R , but for a different source height, H_S' may be approximated by

$$I(H_S', H_D, R) = \frac{f(H_S')}{f(H_S)} I(H_S, H_D, R). \quad (10a)$$

Conversely, the intensity at the same source height, H_S and range R , but for a different detector height, H_D' may be approximated by

$$I(H_S, H_D', R) = \frac{f(H_D')}{f(H_D)} I(H_S, H_D, R). \quad (10b)$$

Figure 3 shows a plot of $f(H_S)$ and $f(H_D)$ versus H_S (or H_D) expressed in mean-free-paths. For sea level air density ($\rho=1.29 \text{ gm/cm}^3$), the mean free path of fission neutrons in air is approximately 81 meters and for fusion neutrons ($\sim 14 \text{ MeV}$) the mean free path is approximately 146 meters. The mean free path is not highly sensitive to neutron energy; modified fission spectra and weapon leakage spectra containing only a few percent fission neutrons have approximately the same effective mean free path as pure fission neutrons.

and a detector height factor, $f(H_D)$, which may be applied to the fluence or the dose $I(R)$ in an infinite air medium to obtain the fluence or dose at the same separation distance (R) but where the source is at height H_S and the detector is at height H_D above the ground:

$$I(H_S, H_D, R) = f(H_S) f(H_D) I(R). \quad (9)$$

The source height factor $f(H_S)$ is the effective fraction of the source leakage neutrons which undergo first collisions in air; hence, it affects equally the multiple scattered neutrons arriving from all directions at a distant detector. It is called an effective fraction because it includes uncollided neutrons which strike the ground but are scattered back out to undergo "first" collisions in air. Similarly, $f(H_D)$ is the fraction (as compared to infinite air) of neutrons which undergo their last collision in air and it includes an adjustment for reflection from the ground in the vicinity of the detector.

If $I(H_S, H_D, R)$ is already known from a transport calculation performed explicitly for H_S , H_D , and R , the intensity at the same detector height, H_D and range R , but for a different source height, H_S' may be approximated by

$$I(H_S', H_D, R) = \frac{f(H_S')}{f(H_S)} I(H_S, H_D, R). \quad (10a)$$

Conversely, the intensity at the same source height, H_S and range R , but for a different detector height, H_D' may be approximated by

$$I(H_S, H_D', R) = \frac{f(H_D')}{f(H_D)} I(H_S, H_D, R). \quad (10b)$$

Figure 3 shows a plot of $f(H_S)$ and $f(H_D)$ versus H_S (or H_D) expressed in mean-free-paths. For sea level air density ($\rho=1.29 \text{ gm/cm}^3$), the mean free path of fission neutrons in air is approximately 81 meters and for fusion neutrons ($\sim 14 \text{ MeV}$) the mean free path is approximately 146 meters. The mean free path is not highly sensitive to neutron energy; modified fission spectra and weapon leakage spectra containing only a few percent fission neutrons have approximately the same effective mean free path as pure fission neutrons.

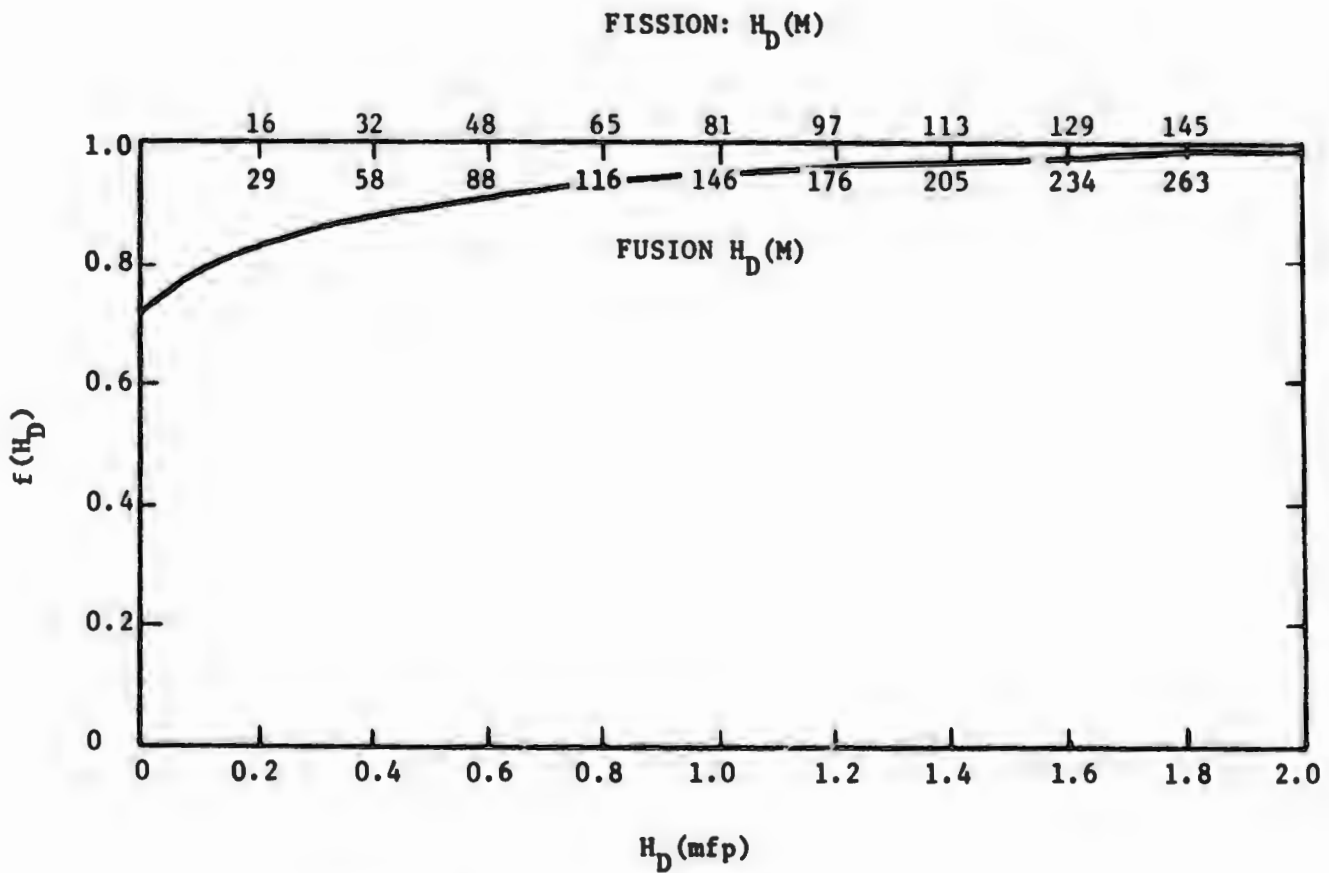
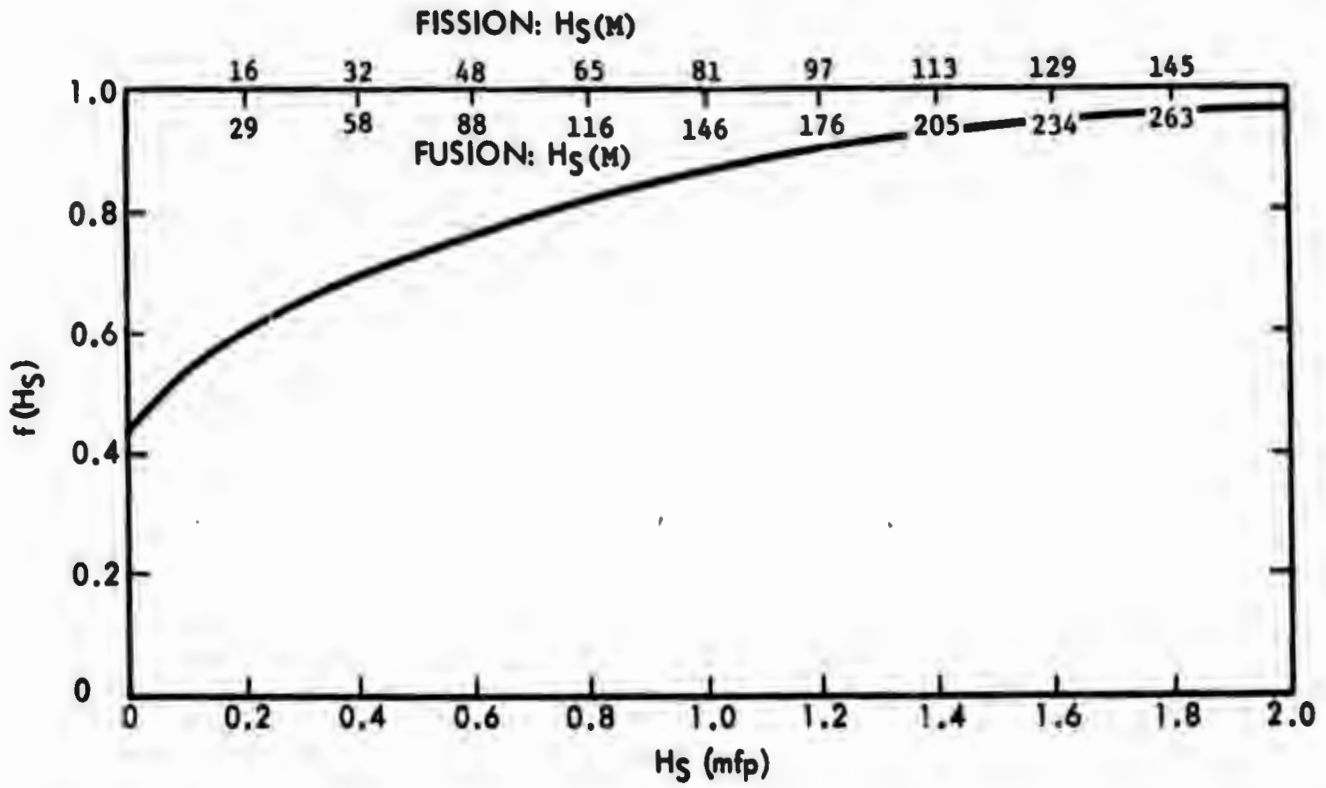


Figure 3. First and Last Collision Fractions

3.2 Secondary Gamma Rays

As described in Section 3.1, the transport of gamma rays produced by neutron interactions in the air and ground was included in Straker's DOT calculations for point isotropic neutron sources 15 meters above the ground. These results, which are the only comprehensive results available to date suitable for generalized application, are included with the neutron data in Table III. They may be applied to specific weapon source terms using the same procedures described for neutrons in Section 3.1.

The secondary gamma rays result from neutron capture and inelastic scattering by the constituents of both air and ground. According to an analysis by Straker which considered results from related Monte Carlo calculations, the relative contribution from the different types of interactions and of air and ground secondaries is highly dependent upon the energy spectrum of the neutron source.⁴ As shown in Figure 4, the gamma ray dose from inelastic scattering is dominant for a fusion-like source (12.2 - 15 MeV), and comprises about 80% of the total at distances greater than 200 meters. Ground secondaries are next in importance with those from neutron inelastic scattering dominating close in, and those from thermal neutron capture dominating at the larger distances. Thermal neutron capture in air and intermediate neutron capture in both air and ground are of only minor importance.

With the fission-like BREN neutron source spectrum (the BREN source is a bare reactor¹²), thermal neutron capture in the ground produces approximately one-half of the secondary gamma dose at ranges less than 800 meters, while thermal capture in air produces a similar amount at larger distances. As may be seen in Figure 5, inelastic scattering is unimportant at virtually all ranges from the BREN source.

The magnitude of the secondary gamma dose is also strongly dependent upon the energy spectrum of the neutron source. Figure 6 compares the

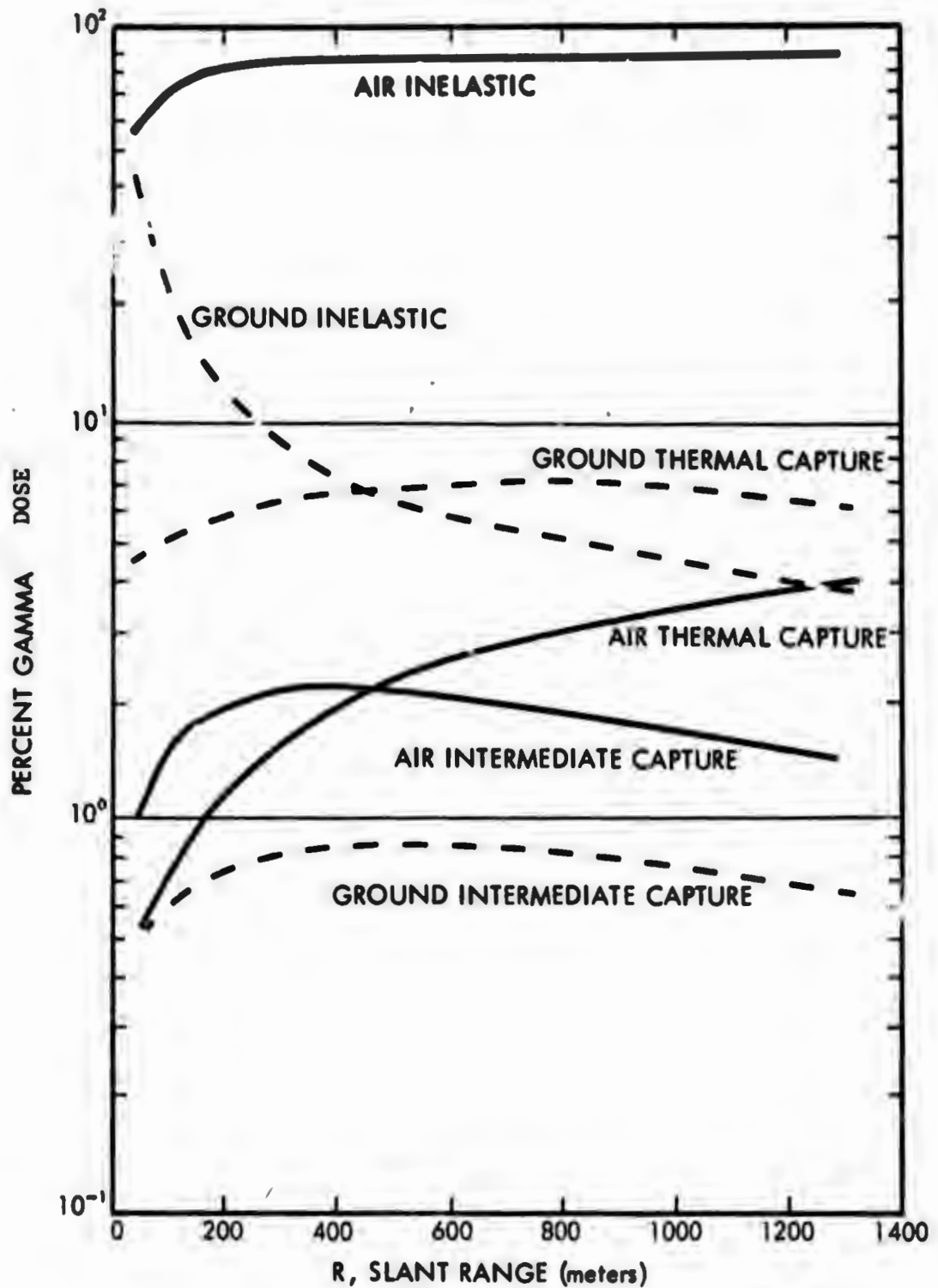


Figure 4. Percentage of Secondary-Gamma Dose vs Slant Range from 14-MeV Neutron Source from Various Reactions in Air and Ground

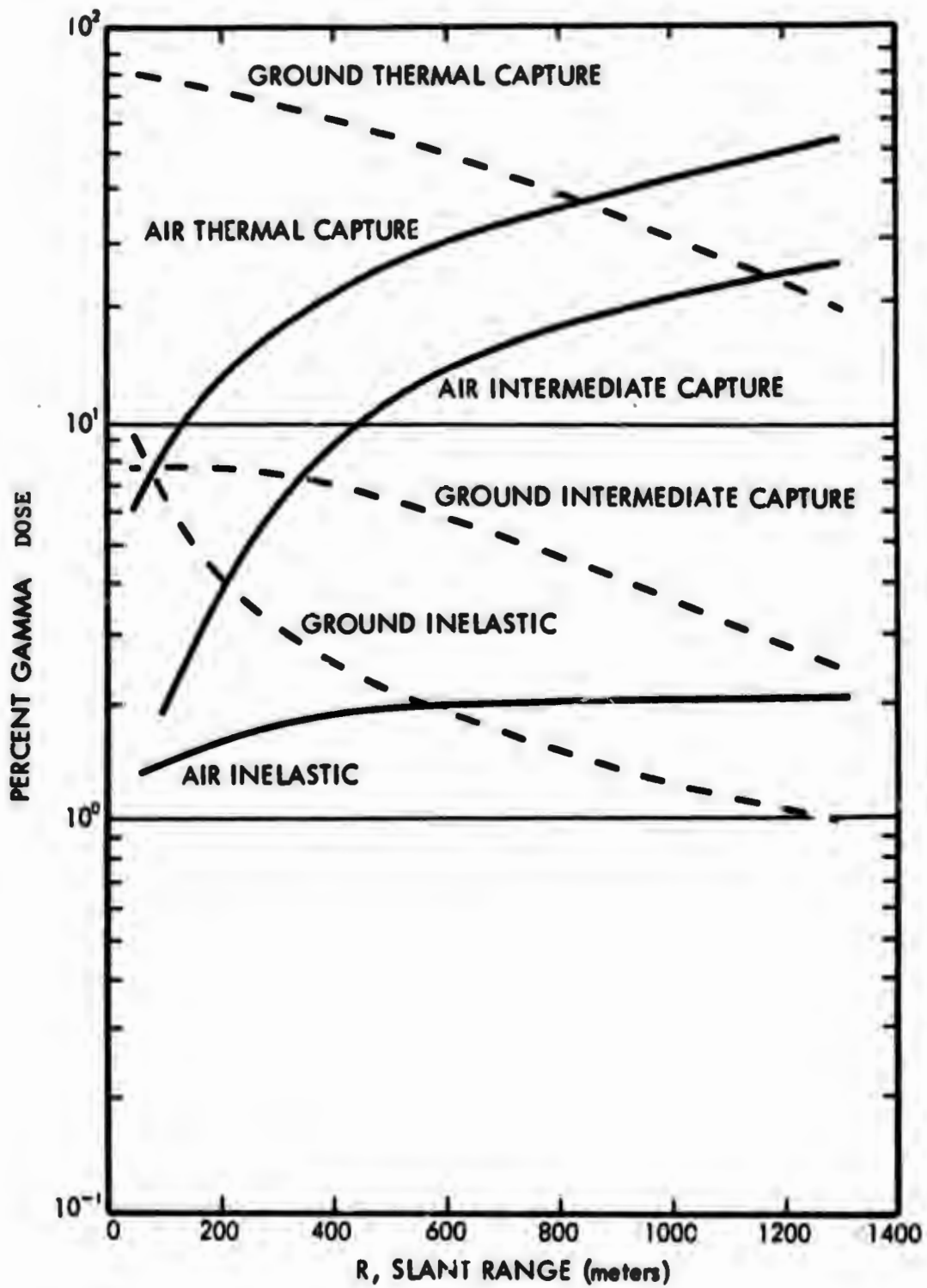


Figure 5. Percentage of Secondary-Gamma dose vs Slant Range from BREN Source from Various Reactions in Air and Ground

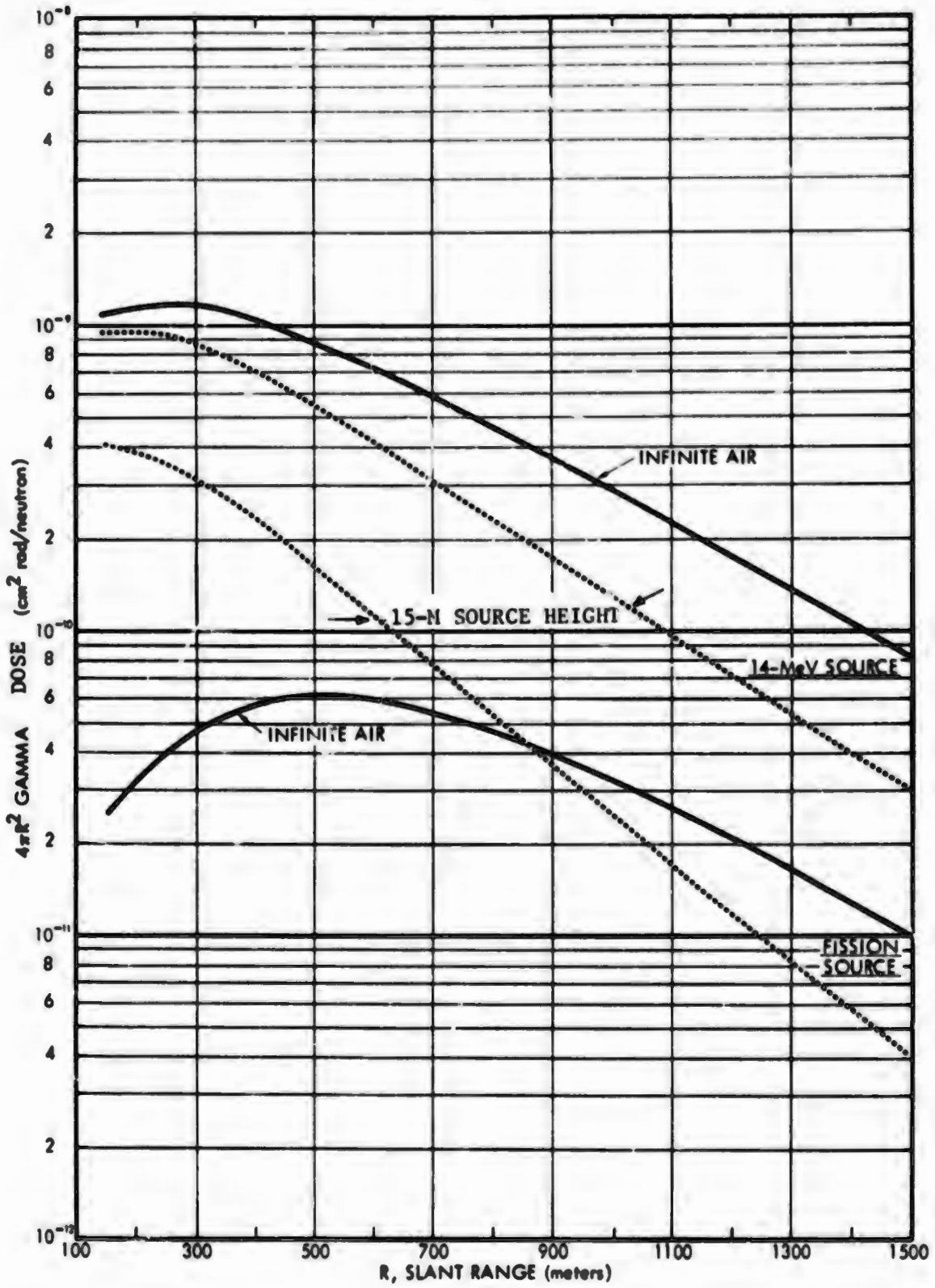


Figure 6. Secondary-Gamma DOSE vs Slant Range for Fission and 14-MeV Neutron Sources

secondary gamma dose versus distance from 12.2 - 15 MeV and fission neutron sources in infinite air and at heights of 15 meters. From this comparison and the ones given above, it seems apparent that the energy spectrum of the neutron source must be taken into account in predicting either the quantity or quality (i.e., distribution in energy and time) of secondary gamma rays.

Another parameter that must be considered is, of course, the number of neutrons leaving the source. The combined effect of differences in neutron source strength and energy spectra is indicated in Figure 7 which shows the secondary gamma dose versus distance calculated for several devices described in Section IV. It is seen that the doses vary as much as an order of magnitude and that the slopes of the curves also depend upon the energy spectrum of the source.

The air-ground interface effect on the secondary gamma rays may be predicted with confidence using the first-last collision method described in Section 3.1 when the neutron source consists largely of high-energy neutrons. The method becomes progressively worse with decreasing neutron energy.⁴ However, in the absence of alternate methods, use of the first-last collision method is probably better than ignoring the interface effect, particularly in adjusting from one source height to another.

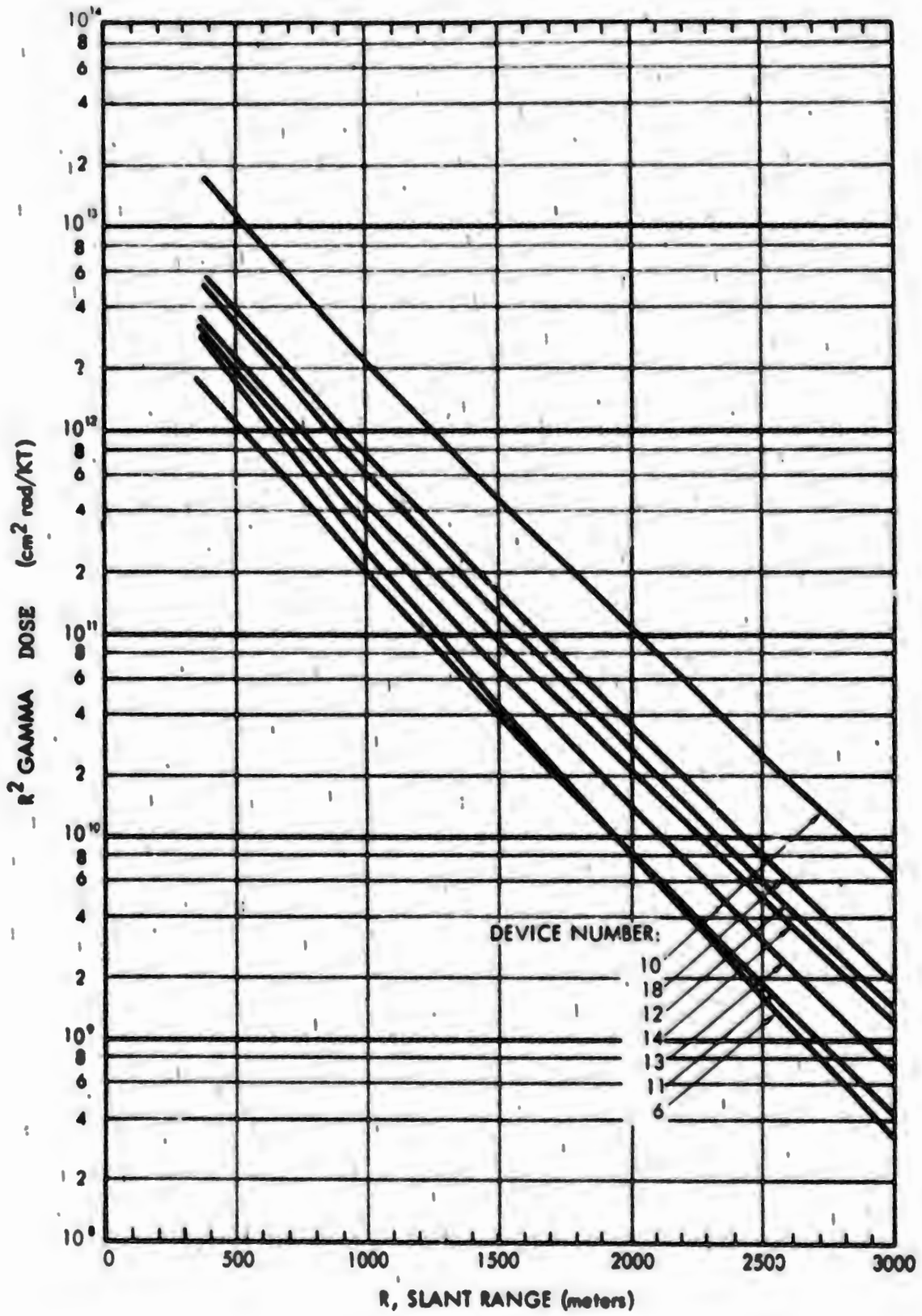


Figure 7. Secondary-Gamma Dose vs Slant-Range for Several Devices

3.3 Fission-Product Gamma Rays

Compared to the neutron problem, the problem of calculating the dose from fission products during the first minute following the detonation of a nuclear weapon is simple in some ways and exceedingly difficult in others.

As discussed in Section 2.3, the quantity and the energy spectrum of the gamma rays from fission-product decay are essentially independent of weapon design whereas the neutrons are strongly dependent. However, the strength, spectrum, height and size of the fission-product source changes during the time interval that must be considered. In addition, the air medium through which the gamma rays are propagated changes drastically with time because of the hydrodynamic effect. The neutron problem, on the other hand, may be treated as static once the neutron leakage from the exploding weapon has been determined.

In developing the fission-product calculation method all of the above mentioned effects plus the air-ground interface effect were considered.⁵ The approach used was to take transport data for a fixed source in a static air medium and introduce approximations to account for the various effects.

Only the effect of the fission-product cloud expansion (source size) and attenuation within the weapon debris of the cloud was found to be negligible for cases of practical interest. Limited sensitivity studies indicated that the fission-product cloud could be treated as a point isotropic source. This approximation is substantiated by the results of a more comprehensive analysis reported in Reference 8.

Gamma Ray Transport Data

Development of the method starts with consideration of the transport

of gamma rays from an idealized point isotropic source of gamma rays in air. Monte Carlo data giving the dose rate versus distance in an infinite air medium for monoenergetic gamma-ray point isotropic sources with energies of 0.5, 1, 2, 4, 6, 8, and 10 MeV have been reported by Marshall and Wells¹³. These data are for an air density of $1.293 \times 10^{-3} \text{ gm/cm}^3$.

For use in the fission-product calculational method, the Monte Carlo data were converted to give the dose per source photon. The results are listed in Table IV.

Source Strength

The air transport data given in Table IV were folded with the fission-product energy spectrum in the 0.2 - 0.5 second time interval following fission. This energy spectrum was taken from the measurements of Engle and Fisher¹⁰ discussed in Section 2.3 and is representative of all gamma rays emitted during the first minute following fission.

As the next step, the resulting data were plotted in the form of R^2 dose per source photon from fission-product decay versus range R expressed in mass thickness or optical depth (gm/cm^2). This curve was fitted by the expression

$$R^2 D(R) = A e^{-R/\lambda} \quad (11)$$

where $A = 3.611 \times 10^{-17}$ and $\lambda = 97.04$ for $R < 21.28 \text{ gm/cm}^2$,
and $A = 5.826 \times 10^{-17}$ and $\lambda = 30.56$ for $R > 21.28 \text{ gm/cm}^2$.

Since $R^2 D(R)$ is the dose (rad) per fission-product source photon, it must be multiplied by the source strength of fission products. Assuming 1.45×10^{23} fissions/KT, a fission fraction F (i.e., fraction of the total yield attributed to fission), a total yield of $W(\text{KT})$ and

Table IV. $4\pi R^2$ Dose from Point Isotropic
Gamma-Ray Source in Infinite Air

(cm^2 rad/source photon)

Source Energy (MeV)	R, Slant Range (Meters)				
	165	640	914	1097	1372
0.5	1.696-10*	6.231-12	5.623-13	8.870-14	9.817-15
1.0	3.017-10	2.405-11	4.150-12	1.170-12	1.148-13
2.0	5.342-10	6.506-11	2.661-11	1.113-11	2.777-12
4.0	9.476-10	2.527-10	1.034-10	5.731-11	2.303-11
6.0	1.270-09	4.242-10	2.136-10	1.271-10	6.014-11
8.0	1.588-09	5.762-10	3.109-10	2.006-10	1.014-10
10.0	2.017-09	7.662-10	4.303-10	2.859-10	1.515-10

*Read 1.696-10 as 1.696×10^{-10}

a time-dependent fission-product gamma-emission rate of $G(T)$ photons/sec-fission, the total source strength (photons/sec) at time T after fission is

$$S(T) = 1.45 \times 10^{23} F W G(T). \quad (12)$$

The decay rate (photons/sec-fission) is represented by a fit to the Engle and Fisher data:¹⁰

$$G(T) = \frac{0.8}{1 + 0.87 T}. \quad (13)$$

Application of these terms to Equation (11) and rearrangement gives the equation for the time-dependent dose (rad/sec) from a stationary point fission-product source in unperturbed homogeneous air (i.e., without the hydrodynamic effect and air-ground interface effect):

$$D(T,R) = \frac{1.16 \times 10^{23} F W A}{(1 + 0.87T)R^2} e^{-R/\lambda}. \quad (14)$$

Three modifications of Equation (14) are required to consider the air-ground interface effect, the cloud-rise effect and the hydrodynamic effect.

Air-Ground Interface Effect

A systematic method for adjusting fission-product gamma ray data for air-ground interface effects is not yet available. However, gamma ray interface effects are relatively small and, consequently, no adjustment or a very crude adjustment may suffice for many purposes. Analysis of BREN measurements¹² and related calculations for ⁶⁰Co gamma rays indicates, for example, that at a separation distance of 730 meters and a source height of 91 meters, the dose at a detector at the ground surface

is 80% of the corresponding infinite air dose. On the basis of these data, a factor of 0.8 was incorporated into Equation (14) as an approximate air-ground interface adjustment.

Cloud-Rise Effect

To account for cloud rise, a time-dependent separation distance, $R(T)$, is substituted for R . $R(T)$ is developed starting with the fitted equation

$$H_C(T) = 61.0W^{0.19}T^{0.82} \quad (15)$$

which gives the cloud height H_C in meters (with reference to the burst height) as a function of time (seconds) following the detonation of a weapon with a yield of $W(KT)$. For a burst height H_B (meters) and horizontal range R_H (meters) to a detector located at the ground surface, the geometric separation distance (in meters) between the center of the rising cloud and the detector is

$$R_G(T) = \sqrt{R_H^2 + (H_C(T) + H_B)^2} \quad (16)$$

For use with Equation (14), R_G must be converted to mass thickness (gm/cm^2):

$$R(T) = 100.0 \bar{\rho} R_G(T) \quad (17)$$

where $\bar{\rho}$ is the ambient air density in gm/cm^3 .

Hydrodynamic Effect

The final modification to Equation (14) is the substitution of a modified mass thickness $R'(T)$ in the exponent to account for the change

in mass thickness of air between the source and detector caused by the hydrodynamic effect. $R'(T)$ is calculated from $R(T)$ as described below. (Note that $R(T)$ must be retained in the denominator of Equation (14), since the geometric distance is not changed by the hydrodynamic effect.)

The modified mass thickness or optical depth is a function of time, yield, ambient air density and pressure, source-detector distance before detonation, and distance at time T after detonation. Several steps are required to calculate $R'(T)$.

First, a scaled distance, J (meters), is given by

$$J = 3.473 \times 10^4 \frac{(qW)^{1/3}}{P} \quad (18)$$

where P is the ambient air pressure in dynes/cm² and $q = 1$ for an air burst (i.e., burst height $> 10^2 W^{1/3}$) and is equal to 2 for a surface burst (burst height $< 10^2 W^{1/3}$). (A value of $q = 2$ was used in the calculations presented in this report.) W is the yield (KT).

The scaled distance, J , is used to calculate a scaled unitless time, L , from

$$L = 0.01183 \frac{P^{1/2}}{\bar{\rho}} \frac{T}{J} \quad (19)$$

where $\bar{\rho}$ is the ambient air density. Two additional quantities, C and V , are calculated from J and L :

$$C = J(0.55974L^{0.31278} + 0.9510L^{1.00025}) \quad (20)$$

when $L < 6.55$,

$$C = J(L + 0.67279) \text{ when } L > 6.55, \quad (21)$$

$$V = 0.95134 + 0.17507L^{-0.68722} \quad (22)$$

when $L < 6.55$,

and $V = 1$ when $L > 6.55$. (23)

A third parameter, Y , is calculated from V by

$$Y = \frac{105(V^2 - 1)}{7V^2 + 35} \quad (24)$$

The effective optical depth (in gm/cm^2) due to enhancement is then calculated from

$$R'(T) = R(T) \left[\frac{21V^2}{56V^2 - 35} \left(\frac{R_o}{C} \right)^Y \right], \text{ when } R_o < C \quad (25)$$

$$R'(T) = R(T) \left[1 - \left(\frac{35(V^2 - 1)}{56V^2 - 35} \right) \left(\frac{C}{R_o} \right) \right], \text{ when } R_o > C \quad (26)$$

where $R(T)$ is the optical depth at time T but neglecting enhancement, as given by Equation (17) and R_o is the original source-detector separation distance calculated from

$$R_o = \sqrt{R_H^2 + H_B^2}, \text{ meters.}$$

The final equation for the total fission-product exposure (rad) during the first T seconds following a detonation, including source decay, cloud rise, the interface effect and the hydrodynamic effect at a range of $R(\text{gm/cm}^2)$ is

$$D(R) = 9.28 \times 10^{22} F W \int_0^T A \frac{e^{-R'(T)/\lambda}}{(1 + 0.87T) R(T)^2} dT \quad (27)$$

Equation (27) and the equations for the various terms were coded for numerical solution by computer. The code was used to calculate the fission-product gamma-ray exposure as a function of range, air

density, weapon yield, and burst height. These calculations were made with and without hydrodynamic enhancement to better determine the importance of the effect.

An example of the output of the code is shown in Figure 8, which illustrates the effects of cloud rise and hydrodynamic enhancement for a nominal 1-KT weapon. It is noted that even for this low yield, the hydrodynamic effect increases the fission-product gamma dose by approximately 50%. However, by coincidence, this increase is almost exactly offset by the cloud-rise effect.

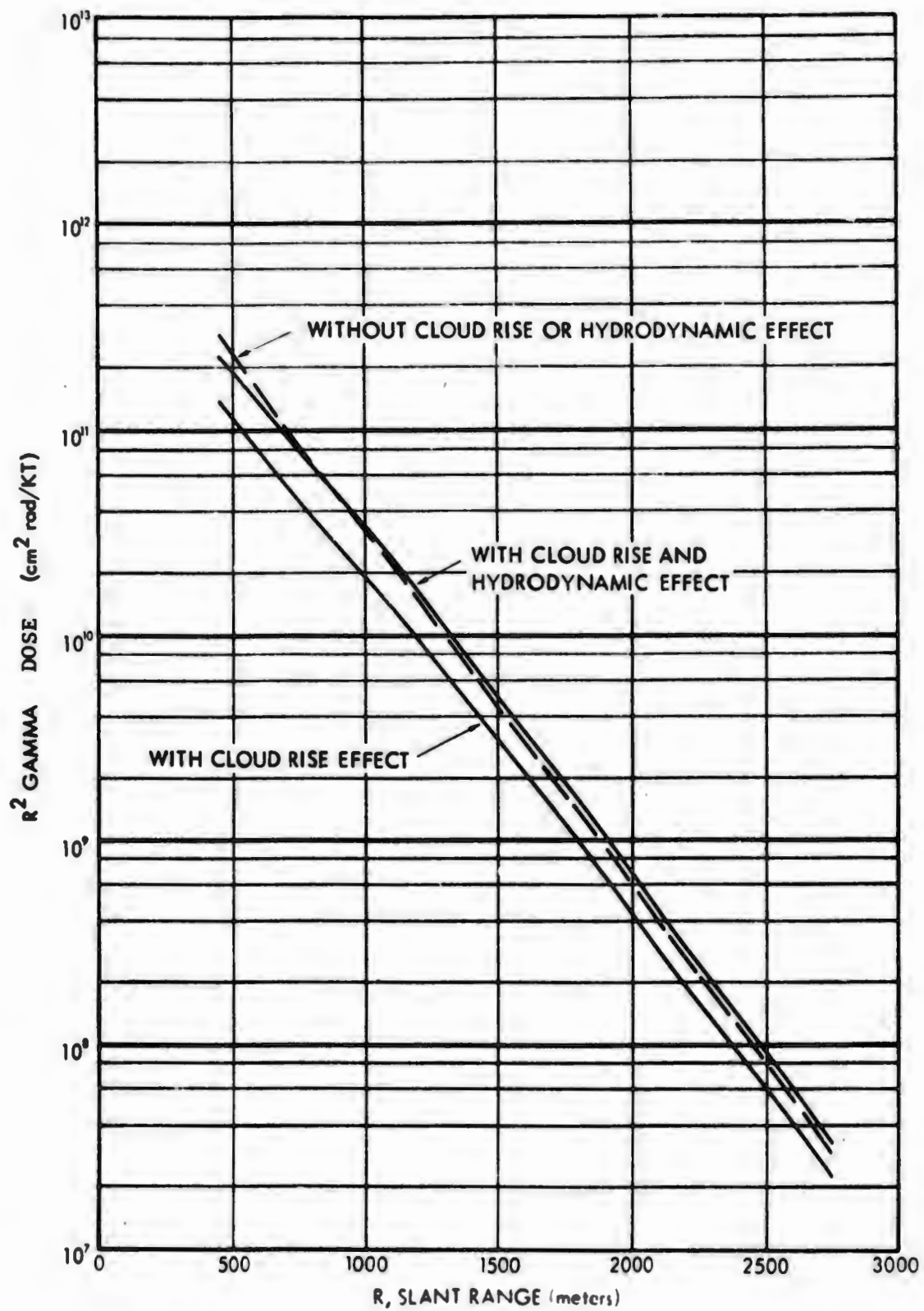


Figure 8. Effect of Cloud Rise and Hydrodynamic Enhancement on Fission-Product Gamma Dose vs Slant Range from Nominal 1-KT Device

IV. METHODS EVALUATION

The data and methods described in the previous section have been validated through comparisons with the results of other calculational methods and with data from field measurements for wide variety of weapon and test devices^{5,6}. The evaluation given here is limited to comparisons with various measurements.

Table V lists an arbitrary identification number and gives the general characteristics of eleven nuclear devices used in the comparisons. These devices, all of which were detonated at the Nevada Test Site or at the Pacific Proving Ground, cover a wide range of yields and detonation conditions. They were selected on the basis of the credibility and completeness of the initial radiation measurements. Another condition imposed on the selection process was that the leakage neutron energy spectrum for the device (or for a similar device) be available for input to the calculations.

Field measurements of the neutron environment from nuclear weapons are subject to a number of uncertainties and it is impractical to verify them by replication. Further disadvantages include the fact that certain types of experimental studies (effect of source height, for example) cannot be performed with a suitable degree of control. Some of these uncertainties and difficulties can be overcome to a certain extent by using nuclear reactors or accelerators designed to simulate the initial radiation from nuclear weapons.

One of the principal weapons radiation simulation experiments performed with a reactor was Operation BREN¹⁴ at the Nevada Test Site. The source was a bare reactor operated at various heights on a 465 meter tower at the Nevada Test Site. Another significant field test using simulated weapon radiation was Operation HENRE^{15,16} also performed at the Nevada Test Site. The HENRE source was a high output accelerator producing 14-MeV neutrons from the D-T reaction and was mounted on the same tower used in Operation BREN.

Table V. Test Devices Selected for Comparison of Calculated and Measured Neutron and Gamma-Ray Dose

Device No.	Nominal Yield (KT)	Weapon Type
6	1	Fission
10	10	Fission
11	35	Fission
12	10	Fission
13	5	Fission
14	20	Fission
18	10	Fission
19	200	Fission
21	500	Thermonuclear
23	1000	Thermonuclear
25	5000	Thermonuclear

4.1 Neutrons

The neutron leakage spectra for the test devices listed in Table V were processed into the 9 source energy bands and folded with the DOT neutron transport data given in Table III for a 15-meter source height using the procedures described in Section 3.1. In addition to doses, Pu, Np, U, and S fluences were calculated for each device using the more complete set of transport data given in Reference 6.

The results were adjusted to the burst height for each test; the actual heights were generally in the range of 100 to 500 meters. The air densities were on the order of 1.0 to 1.05×10^{-3} gm/cm³ for the field tests, but to facilitate intercomparison, all results (both calculated and measured) were adjusted to a common air density of 1.075×10^{-3} .

The final results of the calculations for several of the devices are compared with the measured neutron doses and neutron fluences in Figures 9 through 15. The doses and the S fluences ($E > 2.7$ MeV) calculated using the DOT data generally agree with the measured values within about 25%. The most notable exception among the cases compared is Device No. 6 where the DOT dose values are almost a factor of 2 lower than the measurements at all ranges.

The poorest agreement between the fluences calculated with DOT data and those measured is that for Np ($E > 0.6$ MeV). In virtually every case, the Np measurements are higher than the corresponding calculations. The data measured with the foils having the lower threshold energies tend to be more erratic than the others. However, few individual measurements differ from the calculations by as much as a factor of 2.

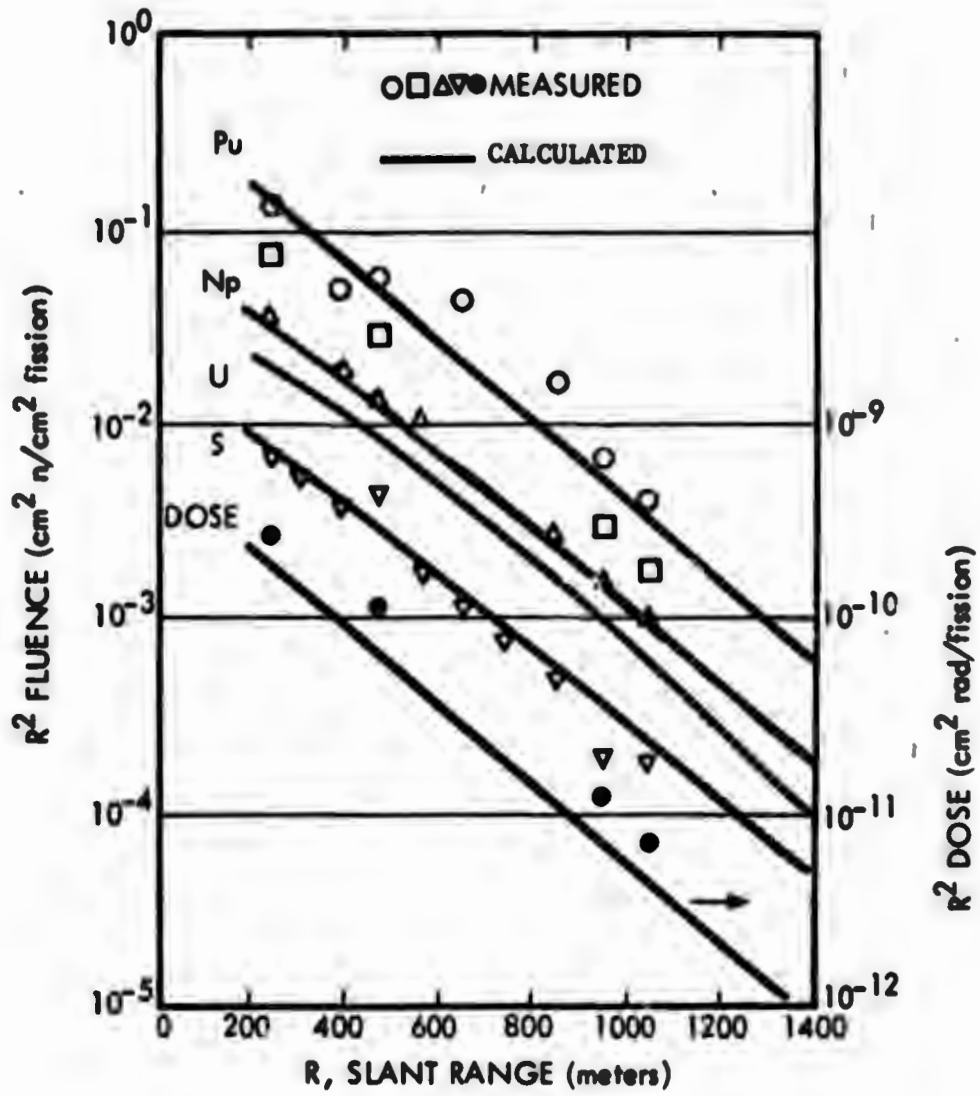


Figure 9. Neutron Activation Fluences and Dose vs Slant Range for Device No. 6

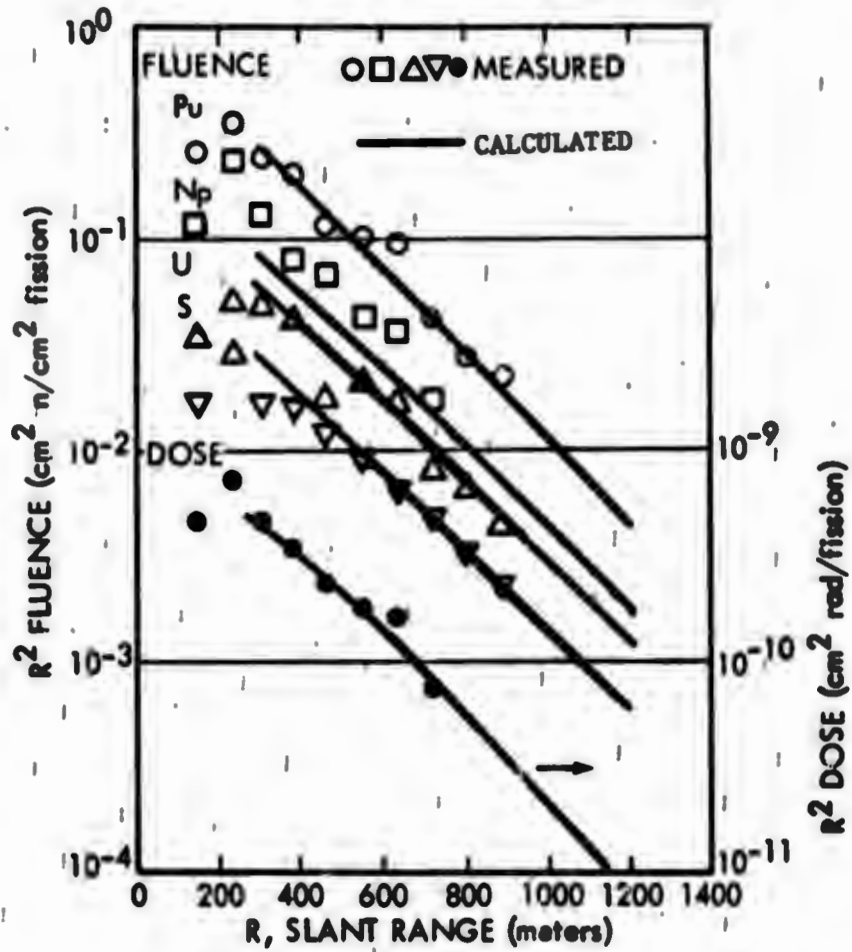


Figure 10. Neutron Activation Fluences and Dose vs Slant Range for Device No. 10

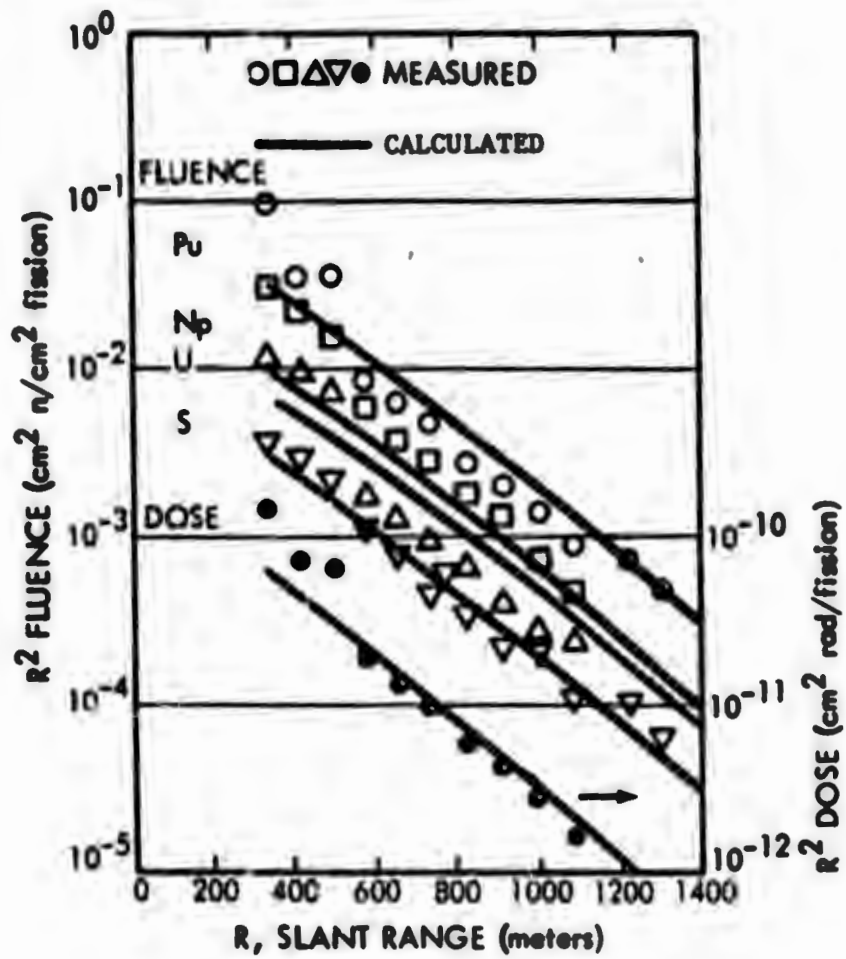


Figure 11. Neutron Activation Fluences and Dose vs Slant Range for Device No. 11

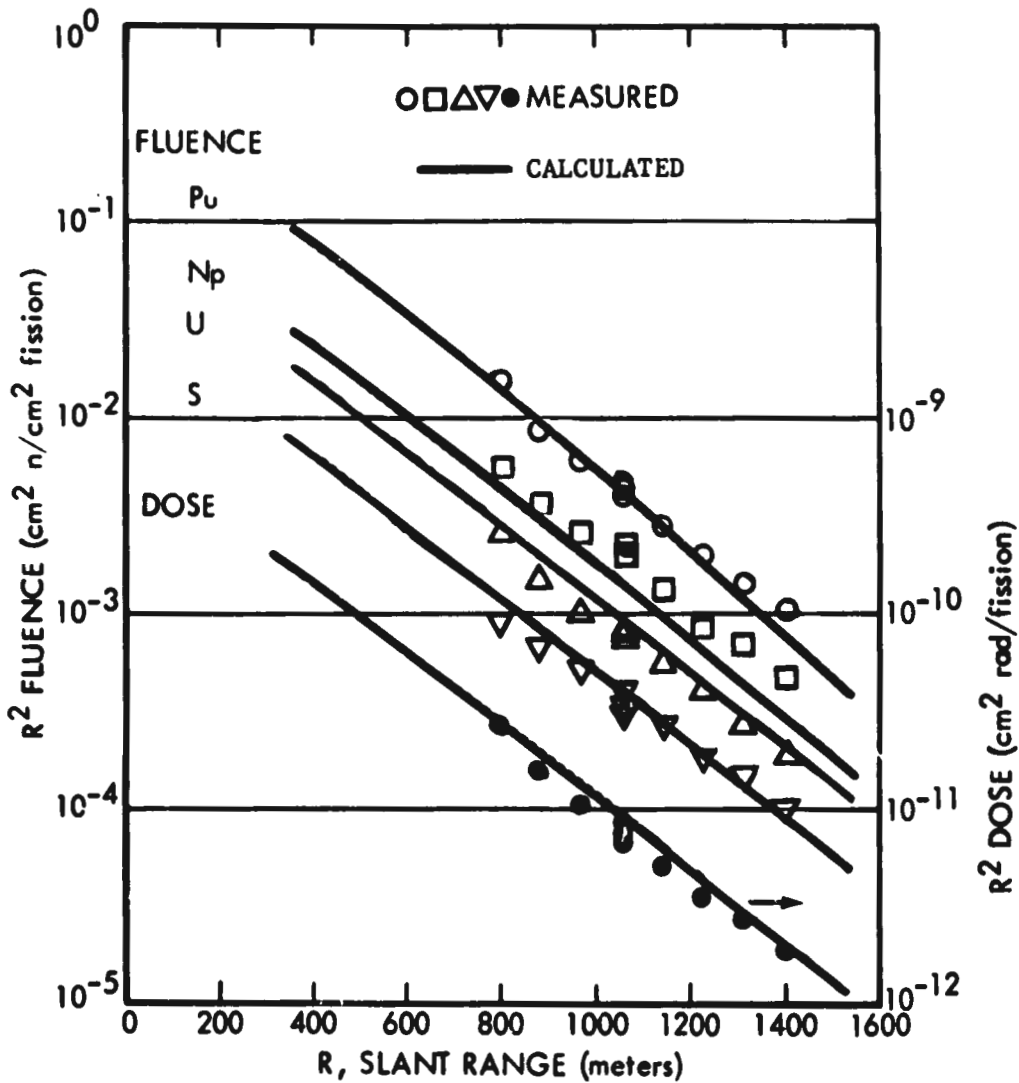


Figure 12. Neutron Activation Fluences and Dose vs Slant Range for Device No. 12

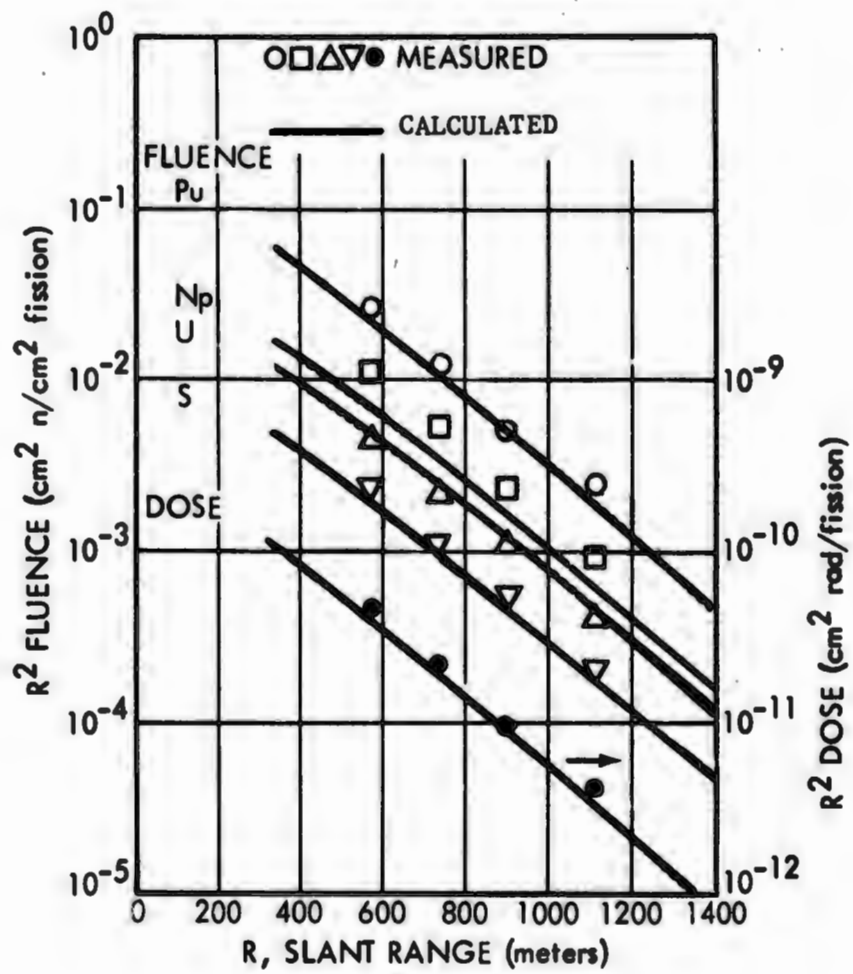


Figure 13. Neutron Activation Fluences and Dose vs Slant Range for Device No. 13

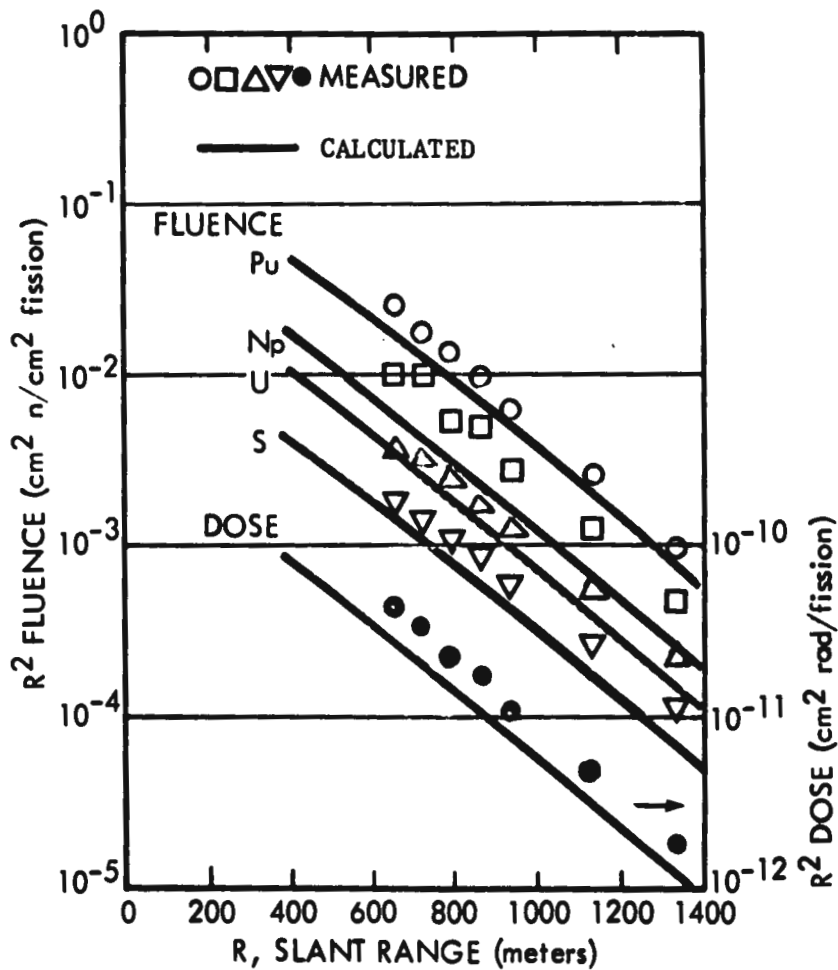


Figure 14. Neutron Activation Fluences and Dose vs Slant Range for Device No. 14

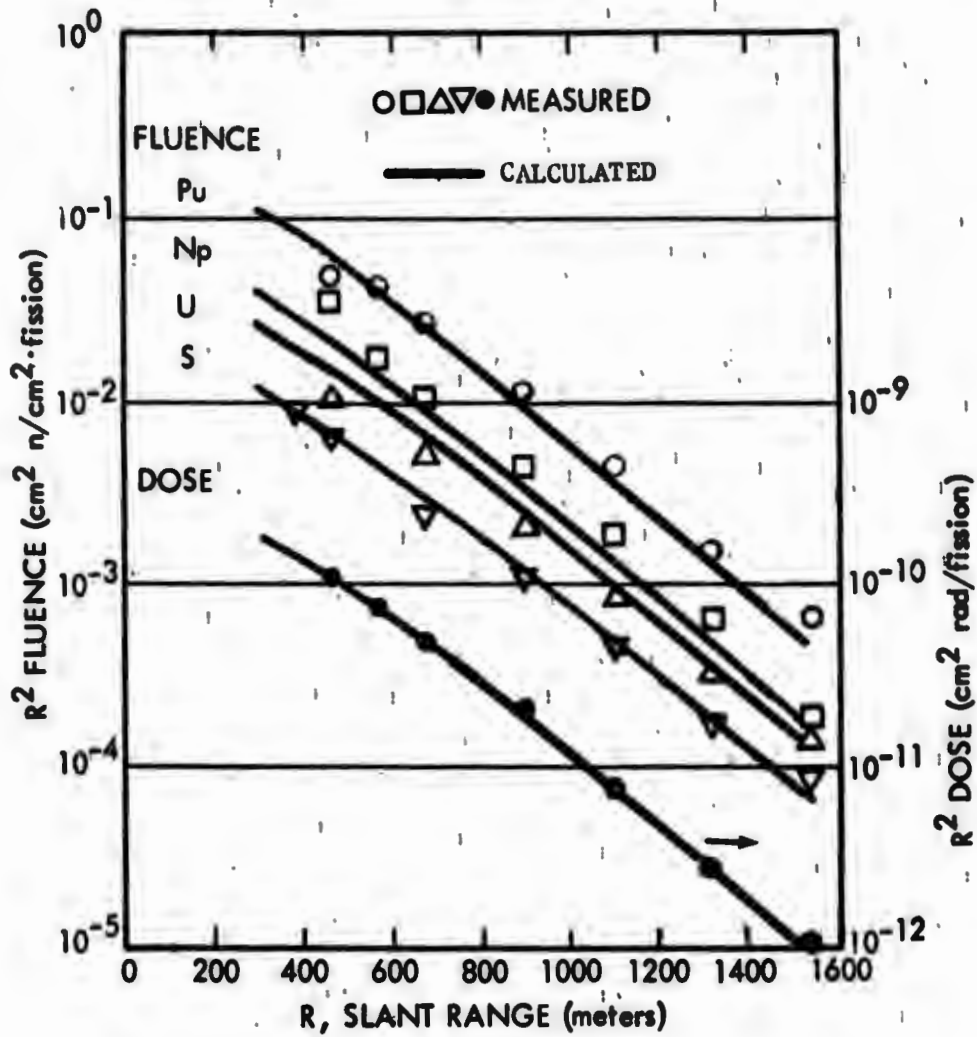


Figure 15. Neutron Activation Fluences and Dose vs Slant Range for Device No. 18

Straker made a special DOT calculation⁴ using the BREN neutron leakage spectrum and a source height of 8 meters for comparison with the measured BREN data.¹⁴ Figure 16 shows the comparison of the calculated and measured neutron dose versus distance. Agreement within 10 to 20 percent is indicated at almost all distances. Included in Figure 16 is a similar comparison of the thermal neutron flux. Since the same procedures and cross sections used in these special DOT calculations were also used in the calculations for monoenergetic sources,¹ the comparisons indirectly substantiate the later calculations.

Data from Operation HENRE^{15,16} include free-field neutron and secondary gamma dose versus distance for various combinations of source and detector height. The measured data were normalized to an effective source strength based on a foil measurement 3 meters beneath the target and the assumption that the target is a point isotropic source. However, mapping measurements made at a distance of 1.5 meters from the center of the target indicate that the source was not isotropic. An analysis of the mapping data was performed to obtain minimum and maximum effective source strengths of an equivalent isotropic source.⁶ These values were used to adjust the measured data before comparing with the calculated data.

Figure 17 compares the adjusted measured neutron dose for an 8-meter source height with that calculated using the DOT data for 12.2-15.0 MeV neutrons. For slant ranges of 80 gm/cm^2 (~ 750 meters), the calculated neutron dose falls within the minimum and maximum values of the measured dose. Beyond 80 gm/cm^2 , the calculated dose is a few percent higher than the maximum measured value. The differences between the measurements and calculations, although not large, seem to be systematic. It is not known whether this is a "real" discrepancy or one resulting from the tedious adjusting procedures necessary to make direct comparisons.

Similar comparisons are included in Figure 17 for measurements made at a source and detector height of approximately 335 meters. The calculated dose is that for in infinite air medium². A significant difference between the slopes of the measured and calculated data is noted.

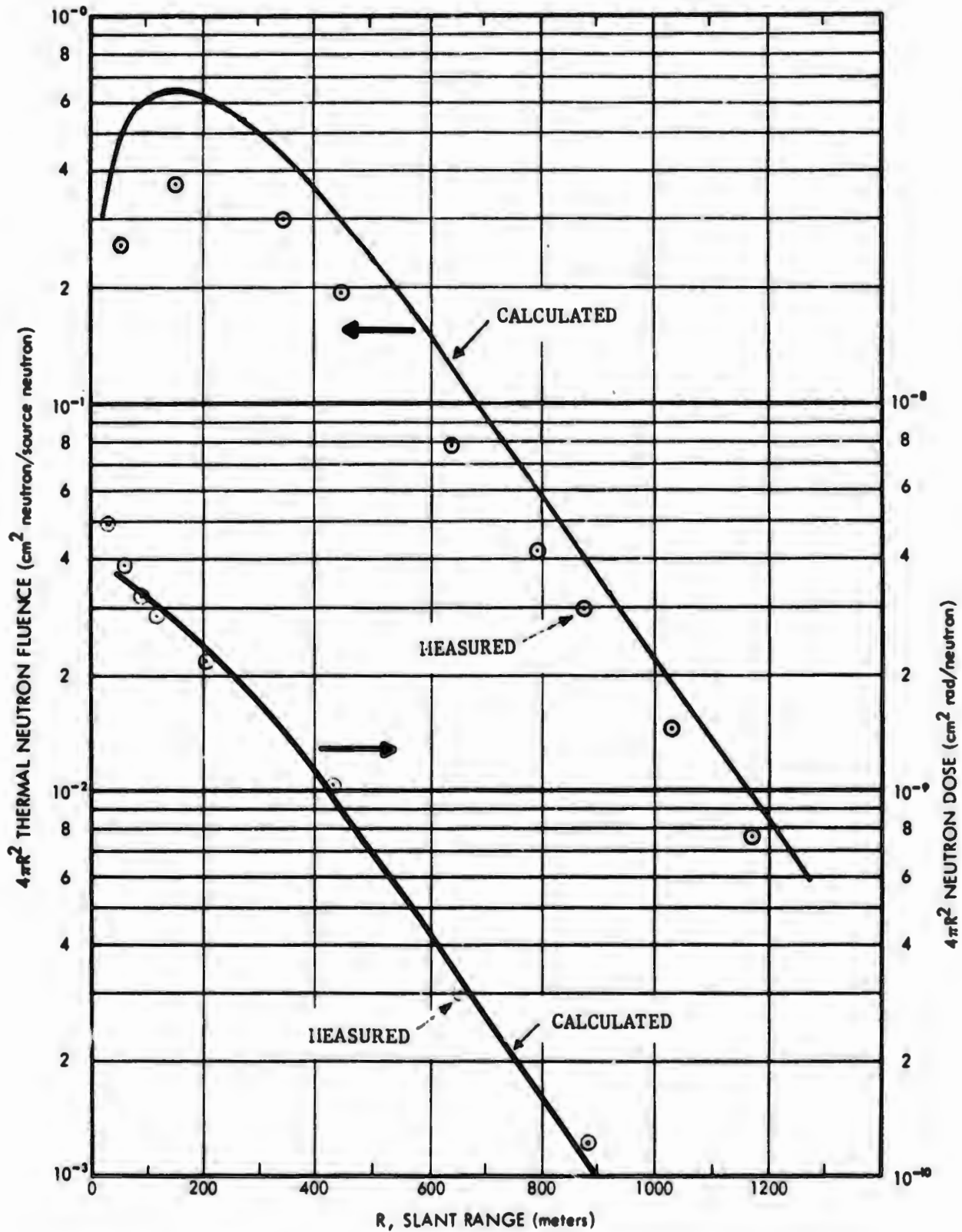


Figure 16. Neutron Dose and Thermal Neutron Fluence vs Slant Range for BREN Source at Height of 8 Meters

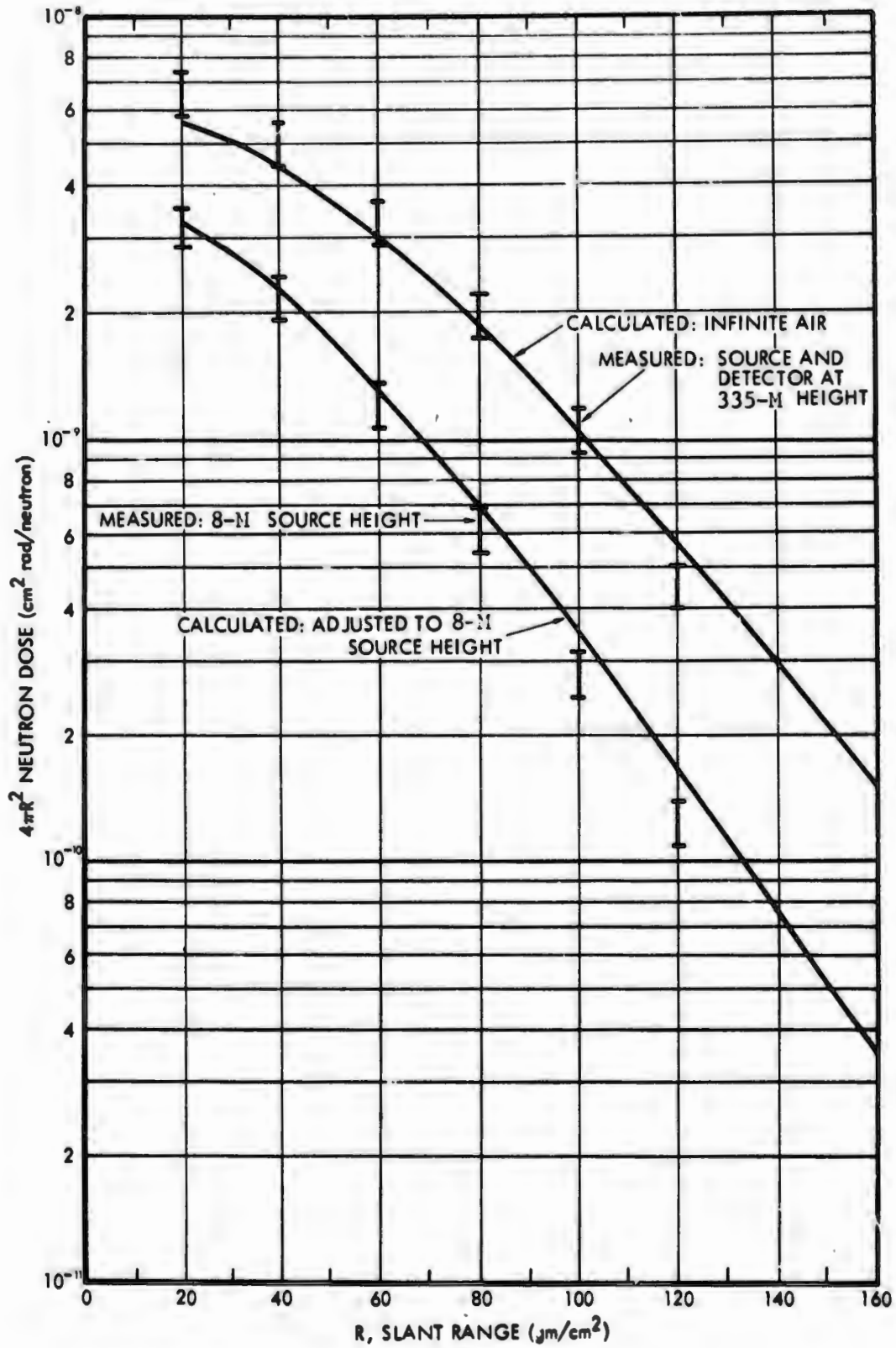


Figure 17. Neutron Dose vs Slant Range for HENRE Source

4.2 Secondary Gamma Rays

There are few sources of data available which allow a direct comparison with secondary gamma doses calculated using Straker's data. All of the measured gamma doses from weapon tests contain fission-product as well as secondary gamma components and comparisons cannot be adequately interpreted unless the fission-product component is known. Section 4.3 provides a number of comparisons of calculated secondary gamma and calculated fission-product gamma ray doses with total measured doses.

As mentioned in Section 4.1 Operation HENRE^{15,16} included measurements of secondary gamma rays produced in air by the 14-MeV neutrons from the accelerator source. The previously described source anisotropy adjustments to the effective source strength were applied to the measured gamma-ray dose spatial distributions to obtain the results for 8- and 335-meter source heights shown in Figure 18.

Included in Figure 18 are Straker's secondary gamma doses for 12.2-15 MeV neutron sources at a height of 15 meters and in infinite air. It is perhaps surprising that the secondary gamma-ray measurements and calculations agree entirely as well as do the corresponding neutron data (see Figure 17). It may be noted, however, that any effects of the source anisotropy not properly accounted for in the adjustments are likely to be less important for the secondary gamma rays.

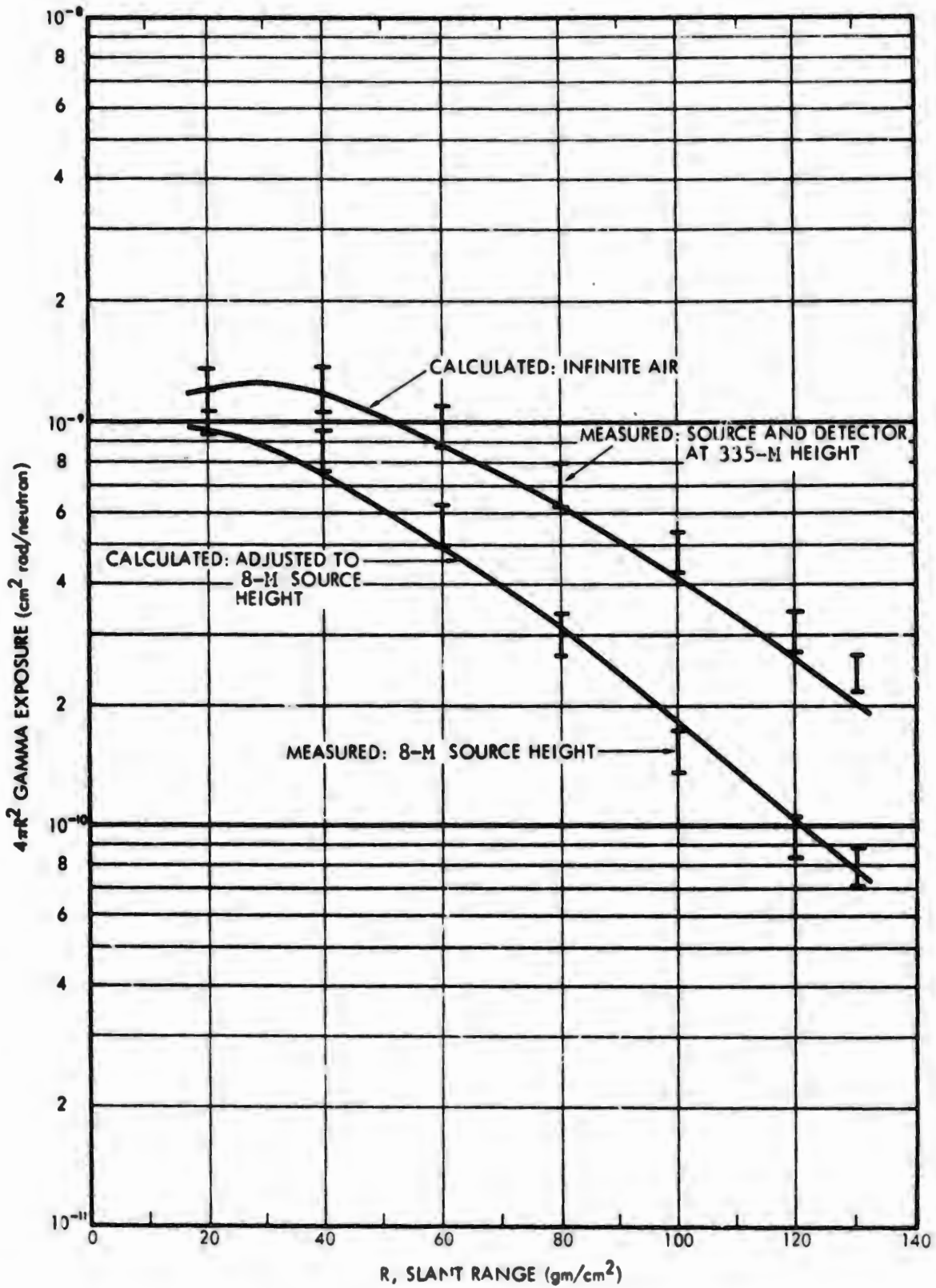


Figure 18. Secondary-Gamma Dose vs Slant Range for HENRE Source

4.3 Fission-Product Gamma Rays

In cases where both the air-ground secondary and fission-product gamma-ray dose are important, both field test data for the weapon and the leakage neutron energy spectrum for the same (or similar) weapon must be available in order to make comparisons. The neutron spectrum is required to calculate the secondary gamma-ray component. Eleven different test events including 7 low-yield devices and 4 high-yield devices (>100KT) which met these conditions are listed in Table V. The low-yield devices include those used in the previous evaluation of neutron predictions (Section 4.1).

Initial gamma-ray calculations were made for each of the 11 devices for the geometrical and meteorological conditions reported during the field tests. The calculations included the fission-product component as given by Equation (27) and secondary gamma-ray component as given by the data and techniques described in Section 3.2.

Low-Yield Weapons

Figures 19 through 25 show comparisons of the calculated air-ground secondary gamma dose, the fission-product gamma dose and the total calculated dose with the measured total doses for seven representative low-yield weapons, all as a function of the slant range from the detonation. The yields of these devices range from approximately 1 to 40KT.

For all weapons except Device No. 10, the fission-product dose is seen to be higher than that resulting from secondaries. The total measured and calculated doses differ most for Devices No. 6 and 10 although the slopes agree favorably. The measured and calculated slopes appear to be somewhat different for Devices No. 11, 13 and 14

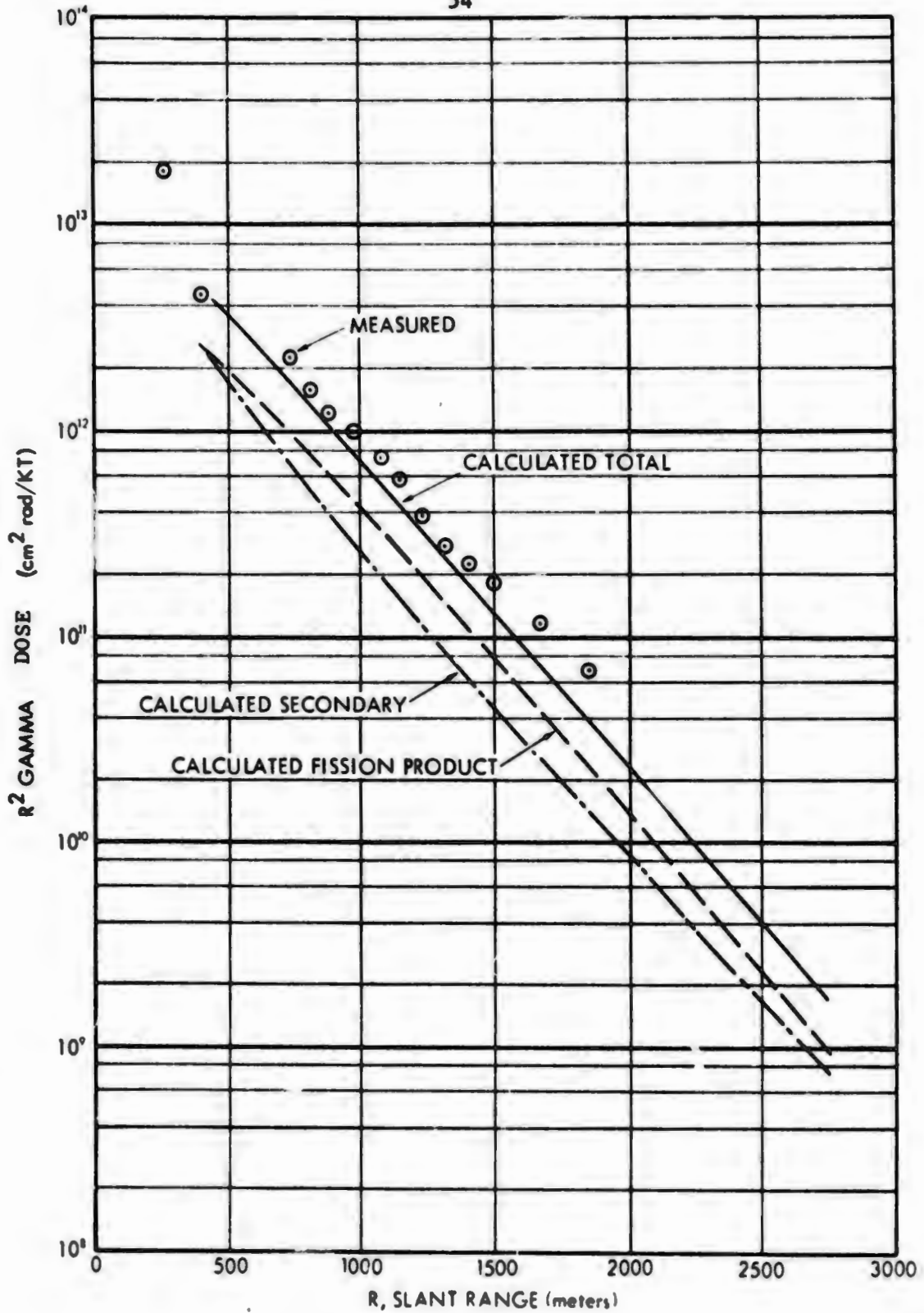


Figure 19. Calculated and Measured Gamma-Ray Dose vs Slant Range for Device No. 6

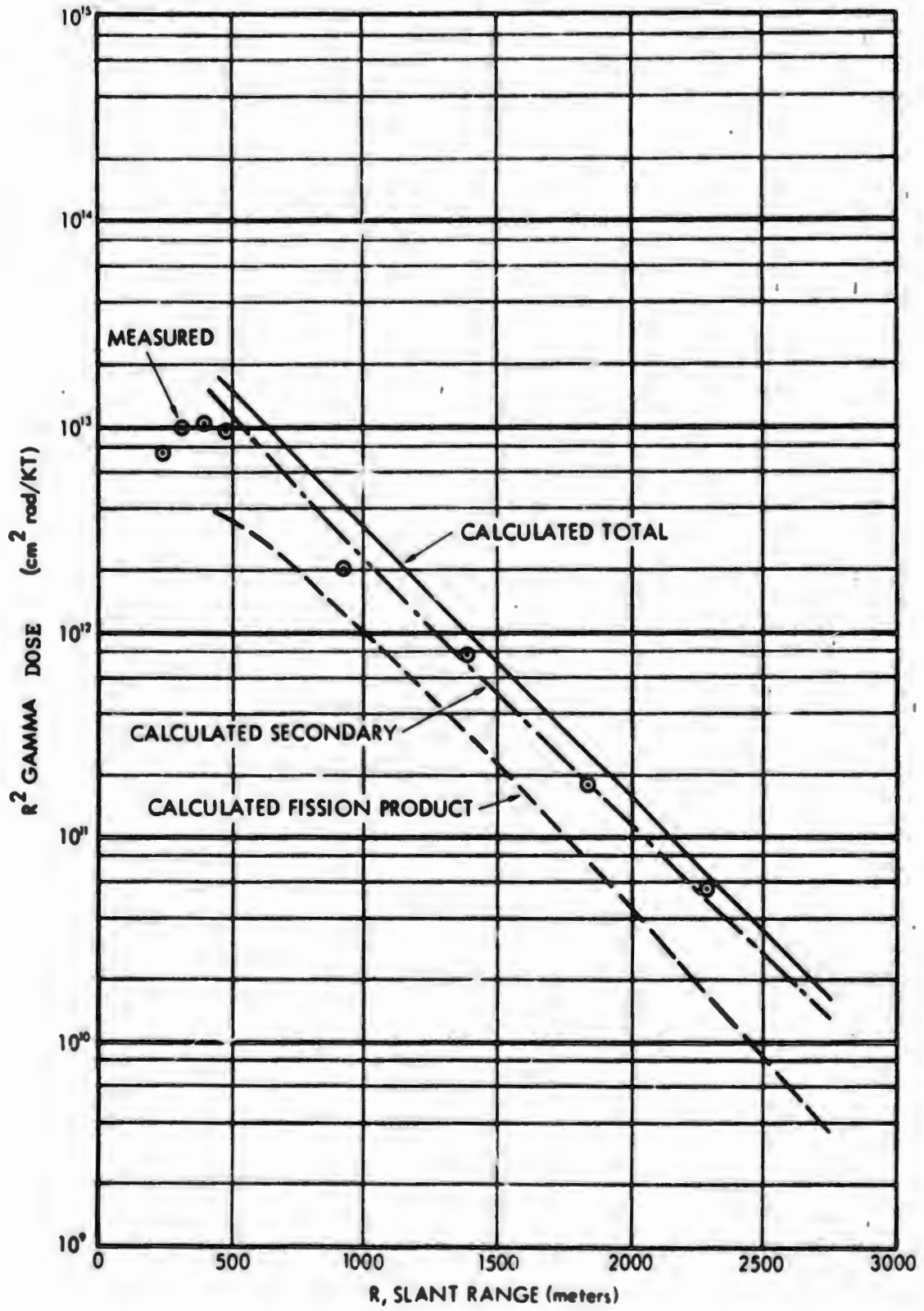


Figure 20. Calculated and Measured Gamma-Ray Dose vs Slant Range for Device No. 10

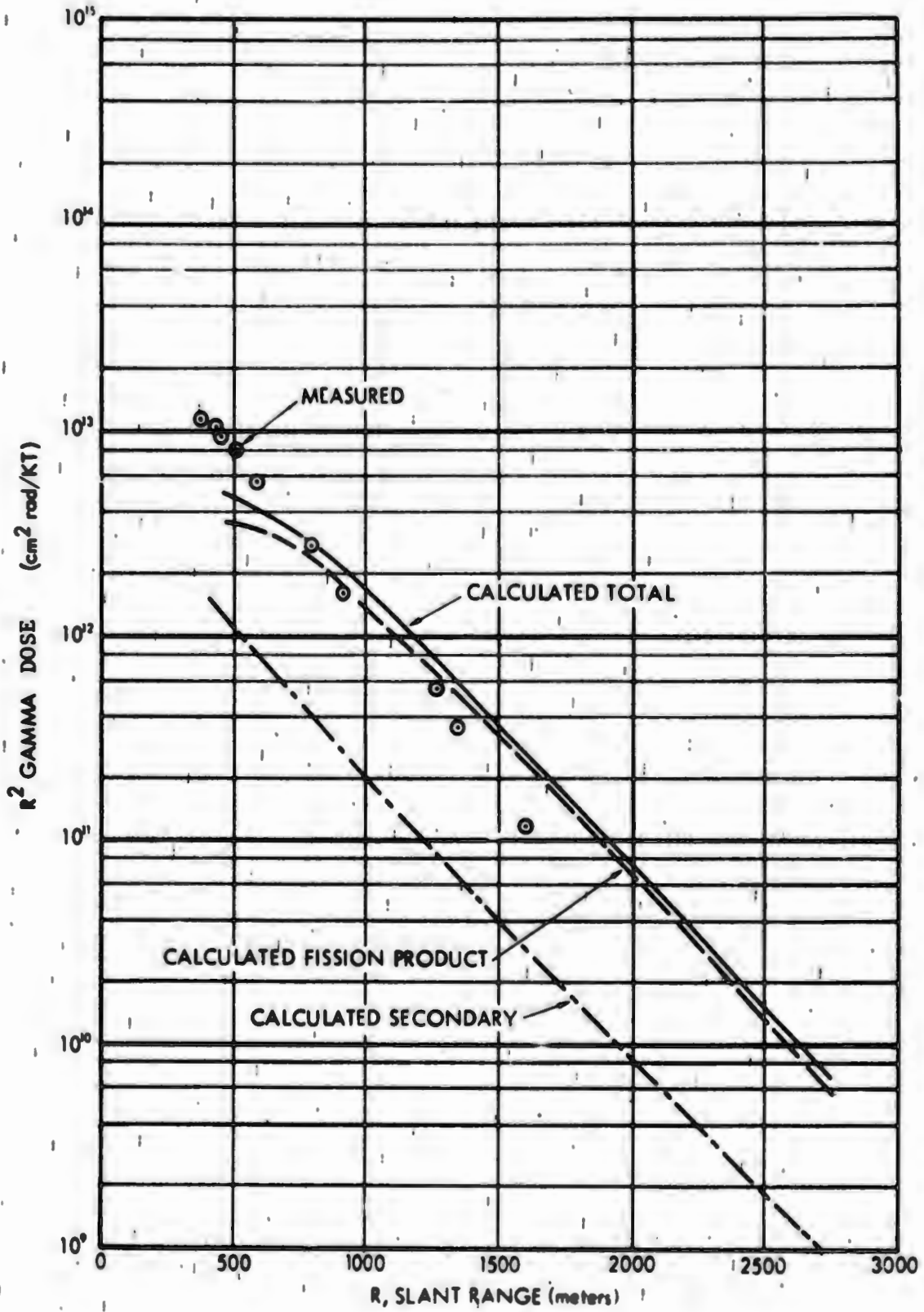


Figure 21. Calculated and Measured Gamma-Ray Dose vs Slant Range for Device No. 11

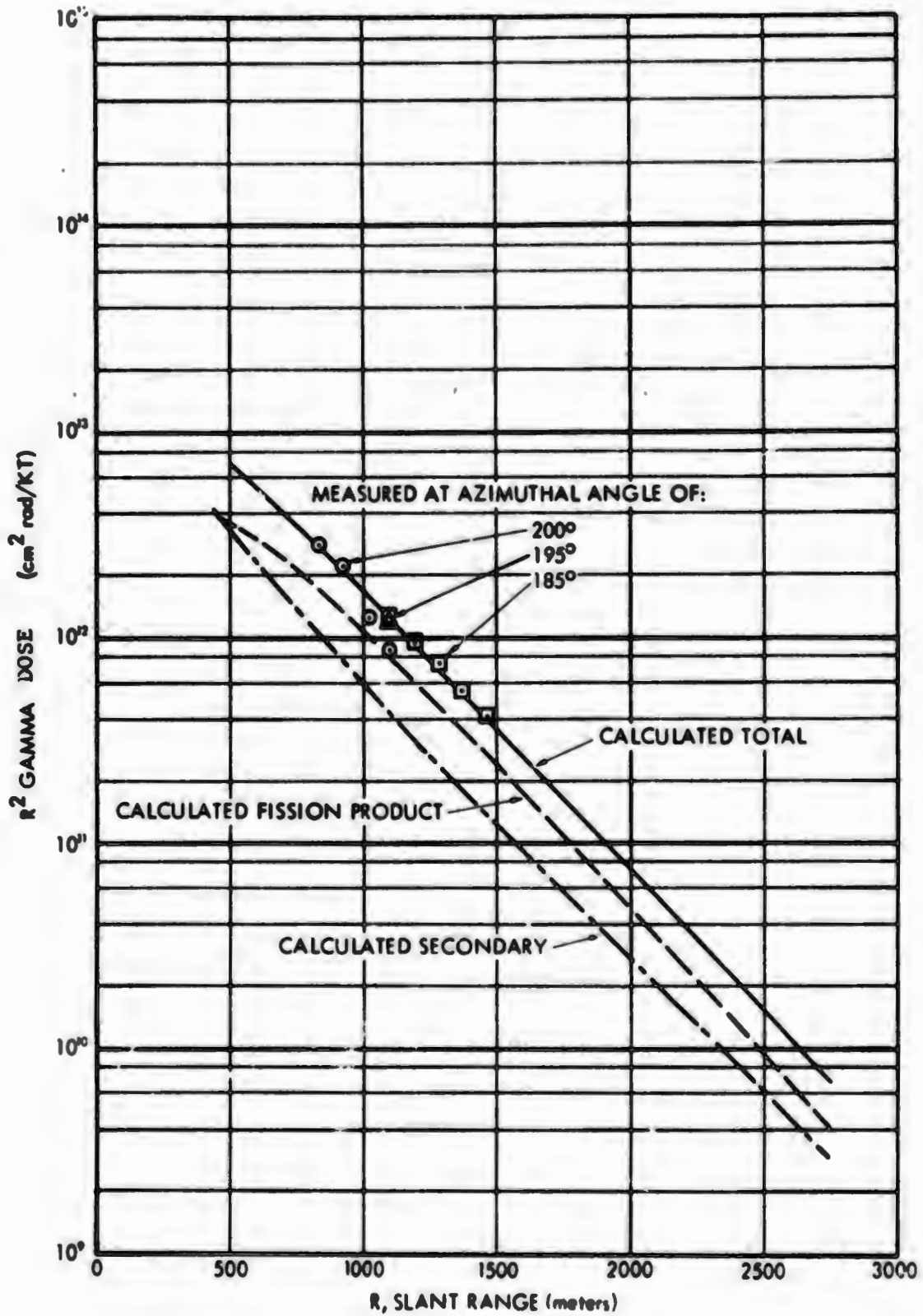


Figure 22. Calculated and Measured Gamma-Ray Dose vs Slant Range for Device No. 12

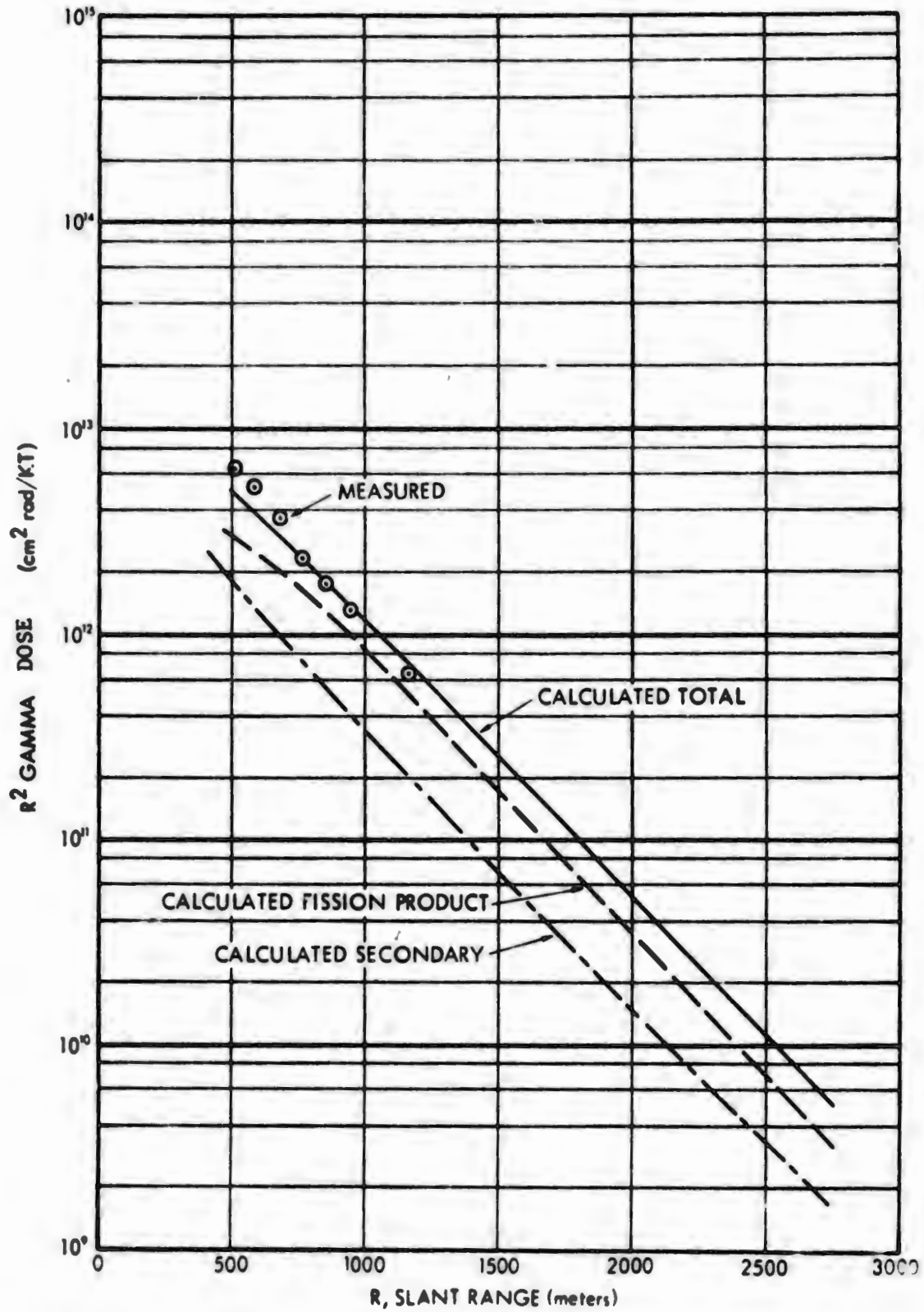


Figure 23. Calculated and Measured Gamma-Ray Dose vs Slant Range for Device No. 13

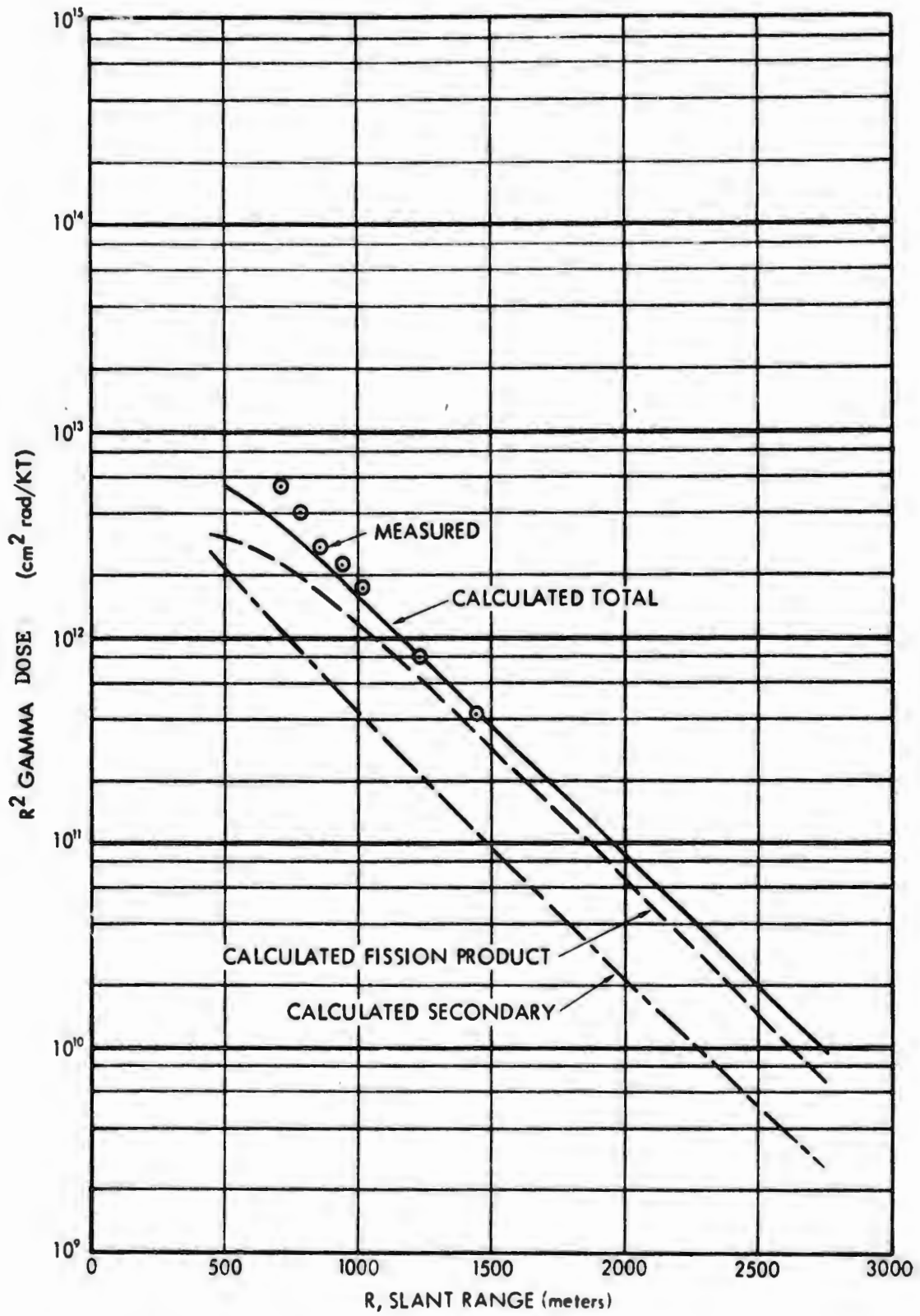


Figure 24. Calculated and Measured Gamma-Ray Dose vs Slant Range for Device No. 14

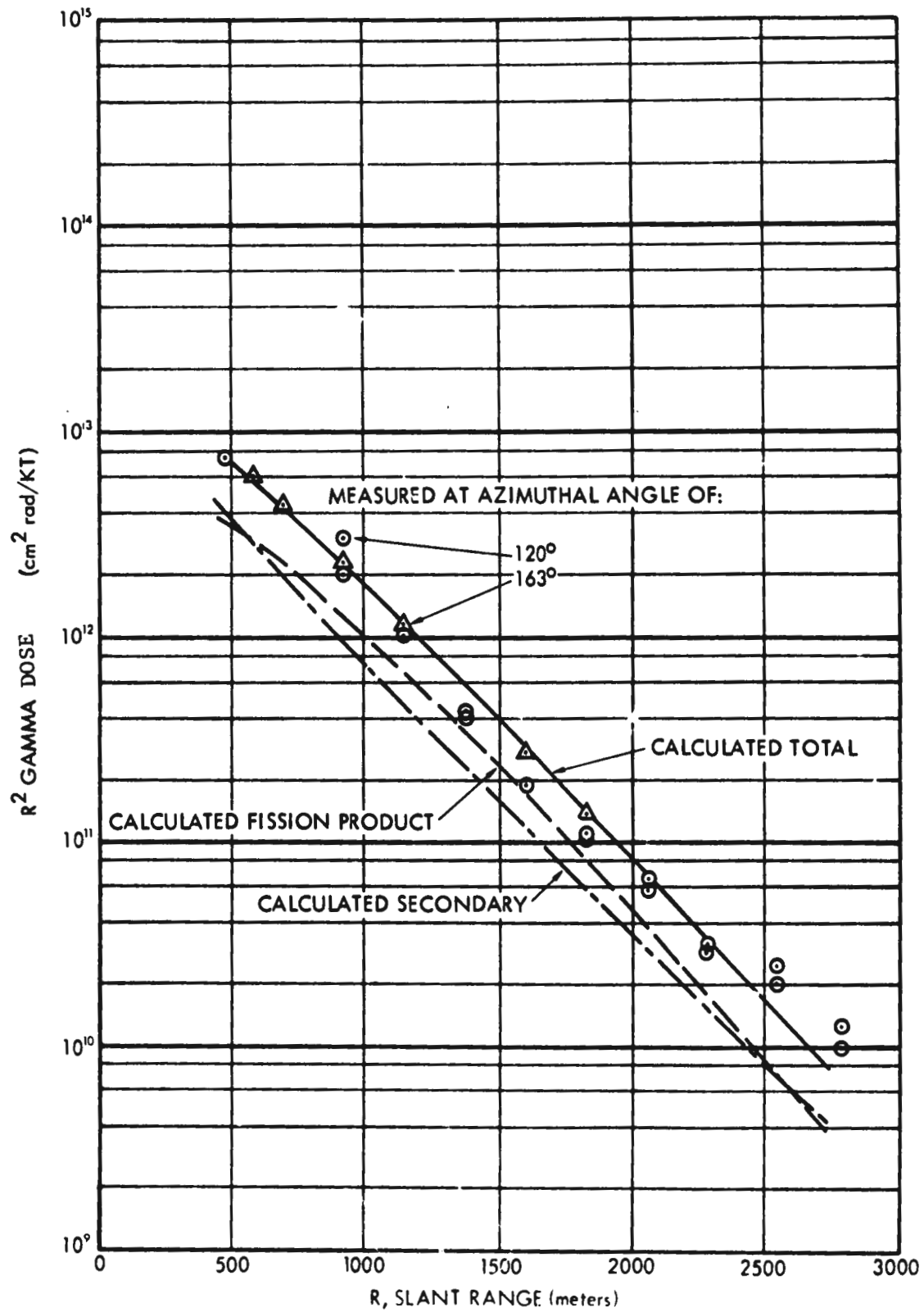


Figure 25. Calculated and Measured Gamma-Ray Dose vs Slant Range for Device No. 18

although most measured points are well within 50% of the calculated totals. The calculations and measurements for Devices No. 12 and 18 are seen to be in generally excellent agreement both in magnitude and slope. The largest area of disagreement is at the short ranges where the neglect in the calculations of cloud expansion and fission-product dispersion through the cloud is least justified.

The overall agreement between the measured and calculated total doses is quite good. Considering all cases compared, approximately 80% of the measured points are within 25% of the calculated totals. As implied by measurements made at different azimuthal angles (see Figure 25, for example), the measured data probably have uncertainties on the order of 25% or more. The differences between the measurements and calculated totals scarcely exceed 50% in the worst cases.

High-Yield Weapons

Figures 26 through 29 show comparisons of the calculated fission-product gamma dose with measurements for four representative high-yield weapons. Leakage neutron energy spectra were not available for these weapons, therefore, the thermonuclear spectrum from Table I was used as a conservative representation of all. The secondary gamma dose on Figures 26 through 29 result from the thermonuclear neutron spectrum and, as can be seen in every case, the secondary gamma dose is less than some 15% of the fission-product exposure. It should be noted that the calculations of the secondary gamma data are for air-over-ground rather than air-over-water, whereas all of the high yield tests were in the Pacific. At present we can only speculate on the difference but it is probably significant.

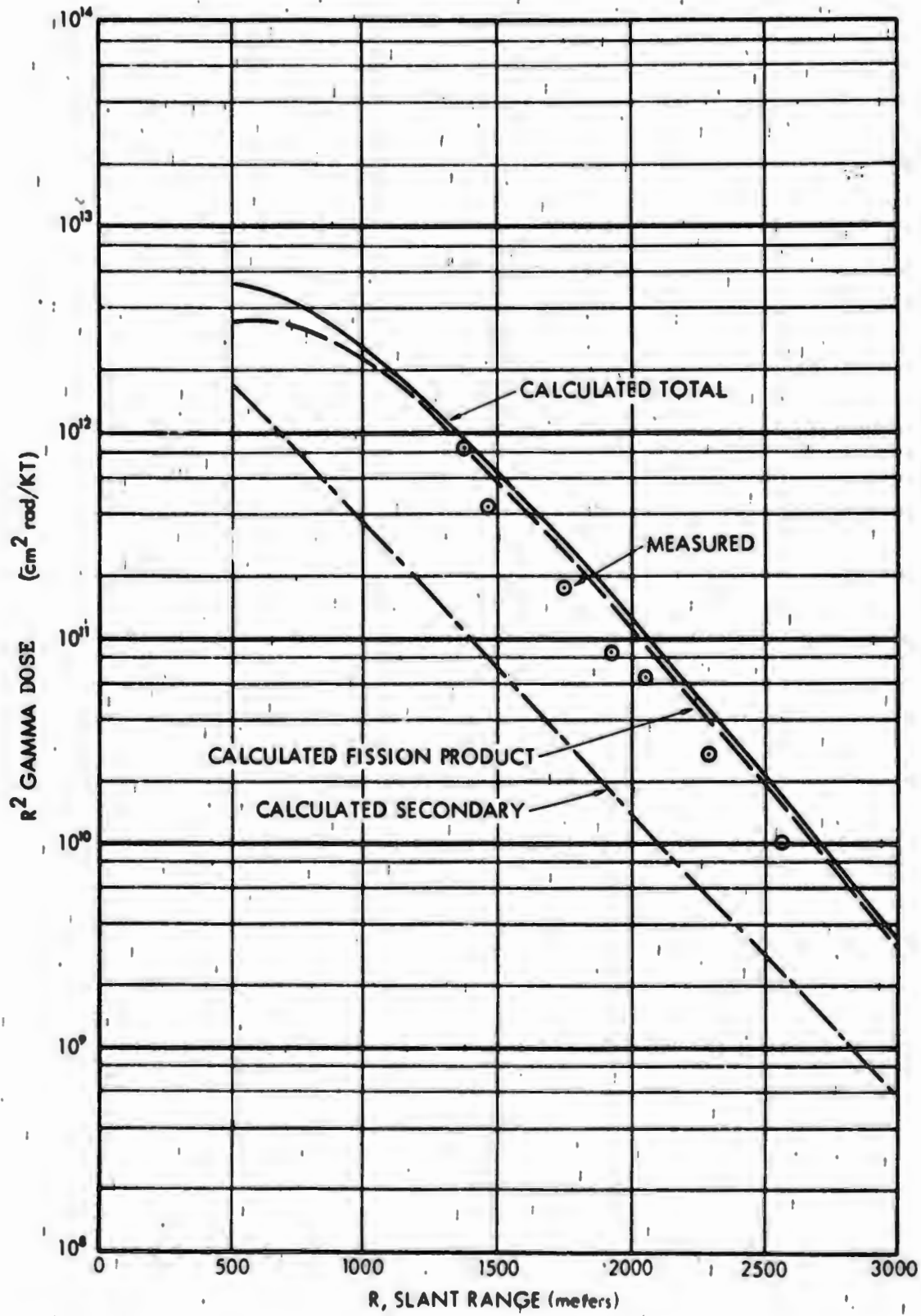


Figure 26. Calculated and Measured Gamma-Ray Dose vs Slant Range for Device No. 19

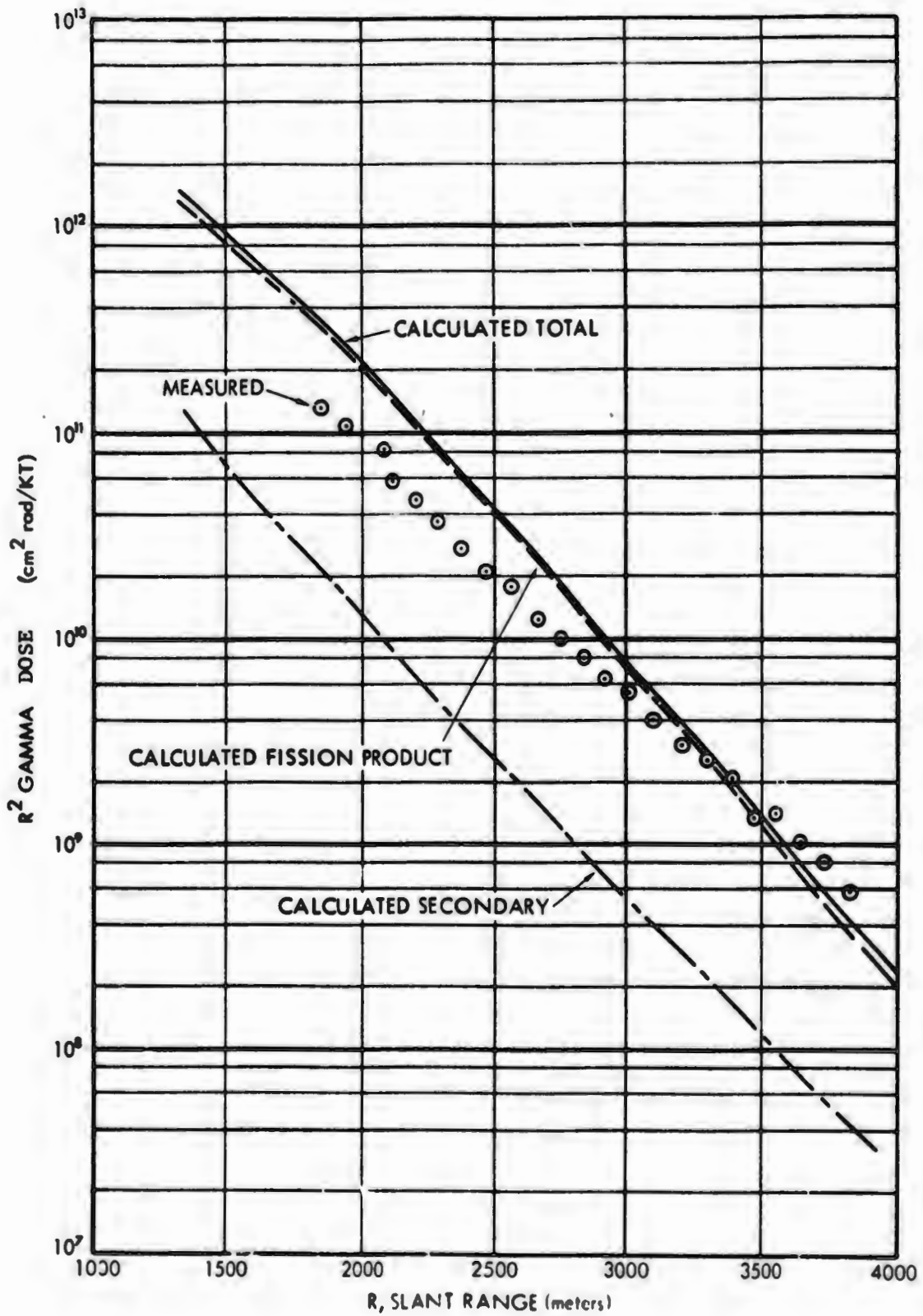


Figure 27. Calculated and Measured Gamma Ray Dose vs Slant Range for Device No. 21

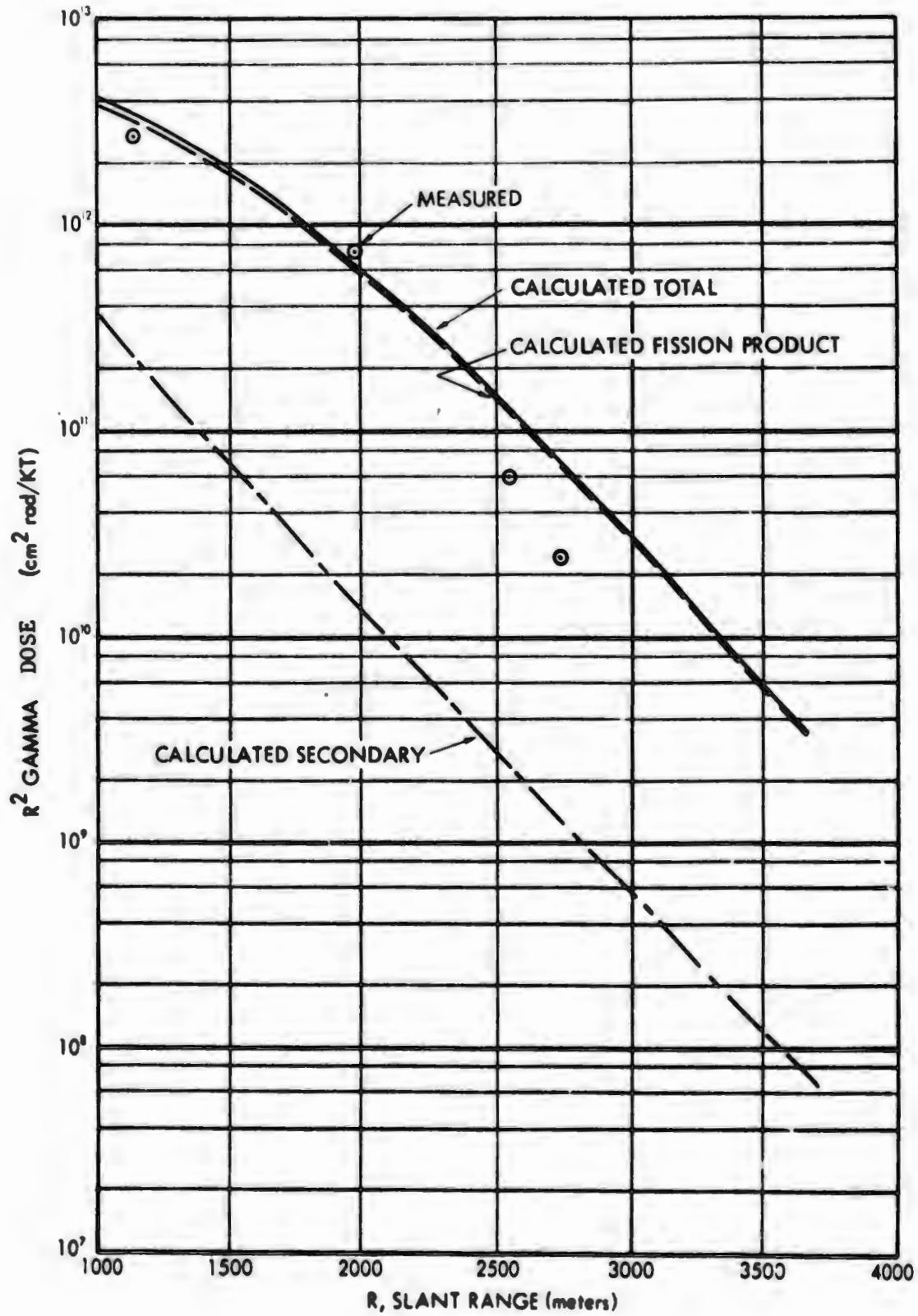


Figure 28. Calculated and Measured Gamma-Ray Dose vs Slant Range for Device No. 23

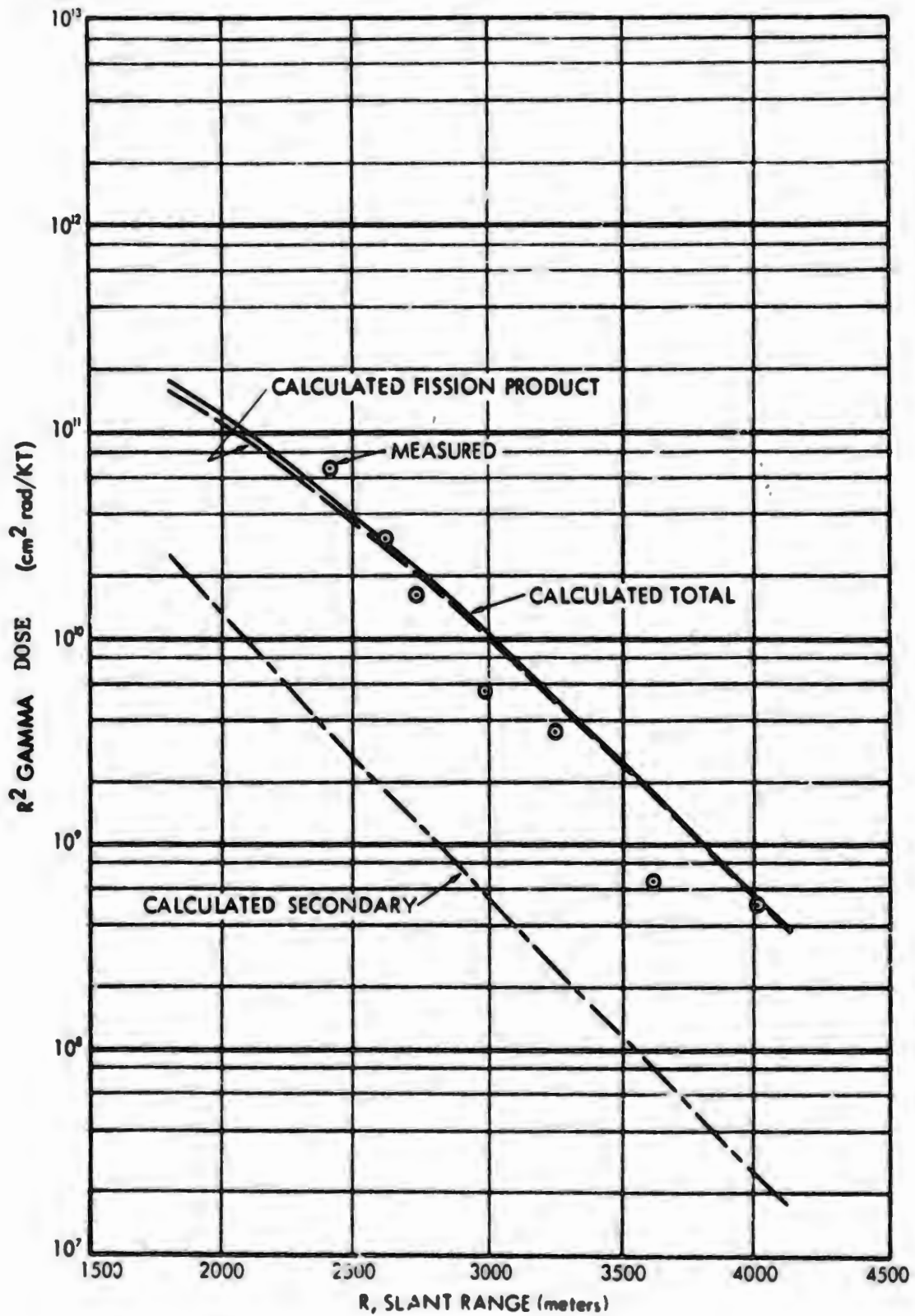


Figure 29. Calculated and Measured Gamma-Ray Dose vs Slant Range for Device No. 25

It is noted that the measured data for the high-yield devices are generally more sporadic than was the case for the low-yield devices. In spite of this, considering all cases compared, approximately 80% of the measured points are within 50% of the calculated total exposures and over one-third agree within 25%. Within the yield range of the high-yield comparisons (approximately 200KT to 5MT), neither total yield nor the fission-to-total yield ratio appears to have a systematic effect upon the agreement between the measurements and the calculations. The fission-to-total yield ratios vary from less than 0.1 to 1.0.

Unlike the calculated doses from the low-yield devices, the high-yield calculated values tend to be higher than the measurements. This is probably due to the attenuation of gammas by the large amount of water pulled up by the surface detonations. This is not included in the calculational models. Although less accurate than predictions for low-yield weapons, the high-yield predictions are more conservative.

V. SIMPLIFIED MODEL

The simplified model provides separate predictions for each of the three principal initial radiation components; neutrons, secondary gamma rays and fission-product gamma rays. The model gives the same results as the detailed calculations for neutrons and for secondary gamma rays provided the weapon of interest is closely represented by one of the three typical weapons included in the model. The model gives fission-product gamma-ray results that agree with the detailed calculations within 20% for low-yield weapons and within 45% for high-yield weapons.

5.1 Charts

Chart 1

The neutron dose per KT of total yield at the ground surface is given as a function of slant range in air with a density of 1.10×10^{-3} gm/cm³ from surface bursts of three representative weapon types. The "fission" weapon is representative of relatively low-leakage pure fission weapons. The "thermonuclear" weapon is a high-yield weapon with a large fusion fraction. The "intermediate" weapon is representative of a high-leakage fission weapon or a low-yield thermonuclear weapon with a low fusion fraction.

To facilitate adjustment to other air densities and to confine the data to a reasonable numerical range, the dose in Chart 1 has been multiplied by R^2 , where R is the slant range. This factor must be removed to obtain the absolute dose. For convenience, a plot of the reciprocal, R^{-2} , is included in Chart 1.

Chart 2

This chart corresponds to Chart 1 in all aspects except that it gives the secondary gamma-ray dose rather than the neutron dose.

Chart 3

The fission-product gamma-ray dose per KT of fission yield at the ground surface is given as a function of slant range in air with a density of 1.1×10^{-3} gm/cm³ from surface bursts of weapons with various total yields. The differences in the dose per KT from the various total yields is caused by the hydrodynamic and cloud rise effects. The 0-KT curve is for a 1-KT yield with no hydrodynamic enhancement and should be used for sub-KT yield weapons.

Chart 4

Scaled slant ranges, R' , are given as a function of actual slant range R , for various air densities. The scaled slant ranges are used for reading doses from Charts 1, 2 and 3 for air densities other than 1.1×10^{-3} gm/cm³. Scaled ranges for air densities not shown may be interpolated from the chart or calculated using the relationship

$$R' = R \frac{\rho}{1.1 \times 10^{-3}}$$

where ρ is the desired air density.

Chart 5

Factors are given for adjusting neutron and secondary gamma-ray doses from Charts 1 and 2 for burst heights above the surface.

Chart 6

Factors are given for adjusting fission-product gamma-ray doses from Chart 3 for burst heights above the surface. The turnover behavior of the curves is due to the interplay between the cloud rise and enhancement effects.

5.2 Equation

The dose D (rad) from each component is given by the same general equation:

$$D = W \cdot D(R) \cdot F(H) \cdot R^{-2}$$

where

W = weapon yield (KT)

(For fission-product gamma rays, W is the fission yield rather than the total yield.)

$D(R) = R^2$ dose per KT at slant range R .

(From Charts 1, 2 and 3 for neutrons, secondary gamma rays and fission-product gamma rays, respectively. If the air density differs significantly from 1.1×10^{-3} gm/cm³, use the scaled range R' from Chart 4 in reading $D(R)$ from Charts 1, 2 or 3).

$F(H)$ = Burst height adjustment factor.

(Chart 5 for neutrons and secondary gamma rays and Chart 6 for fission-product gamma rays).

R^{-2} = Geometric attenuation factor.

(Included in Charts 1, 2 and 3. Note that R is the actual rather than the scaled slant range).

Chart 1. Neutron Dose vs Slant Range from Surface Burst

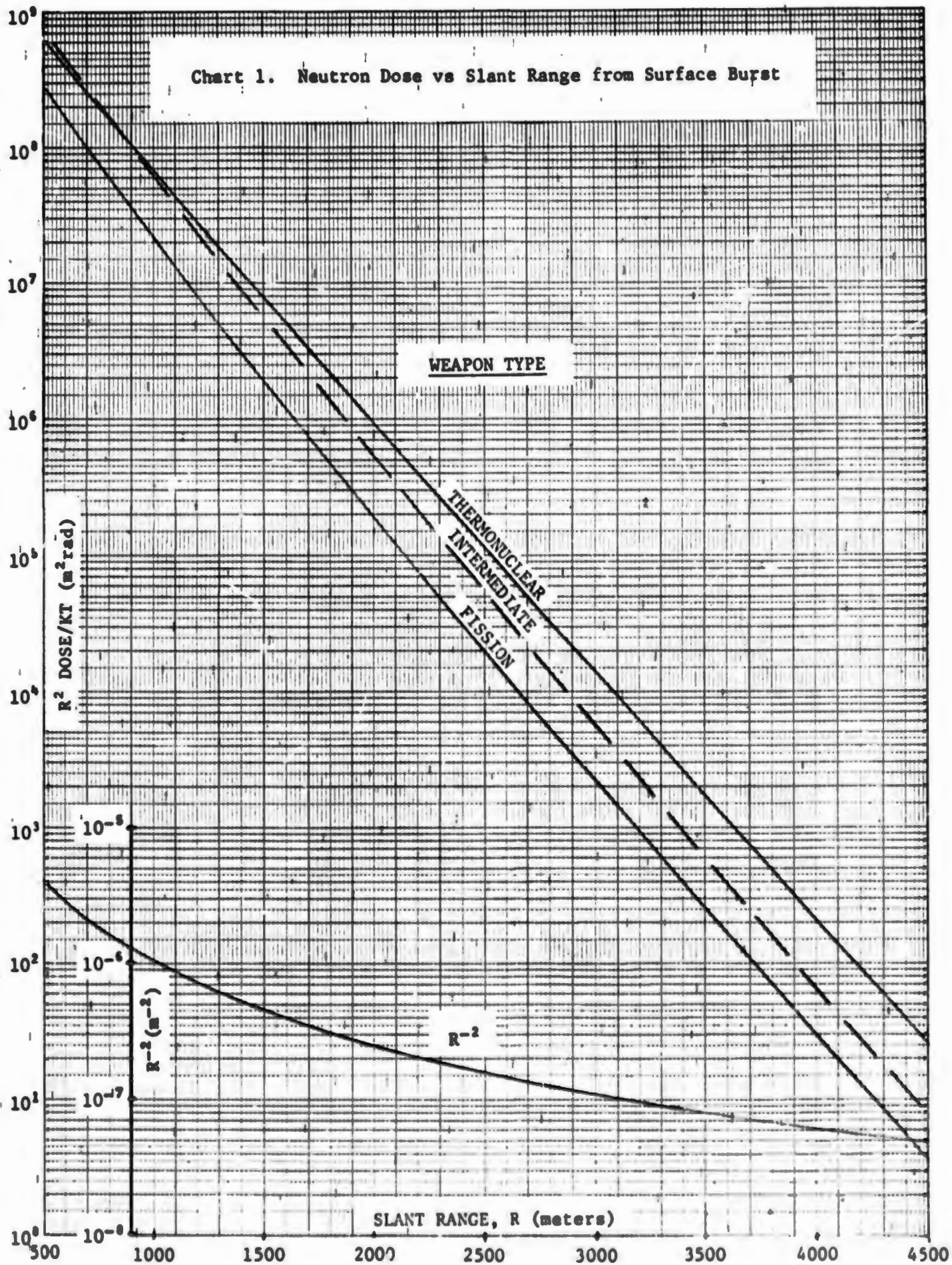
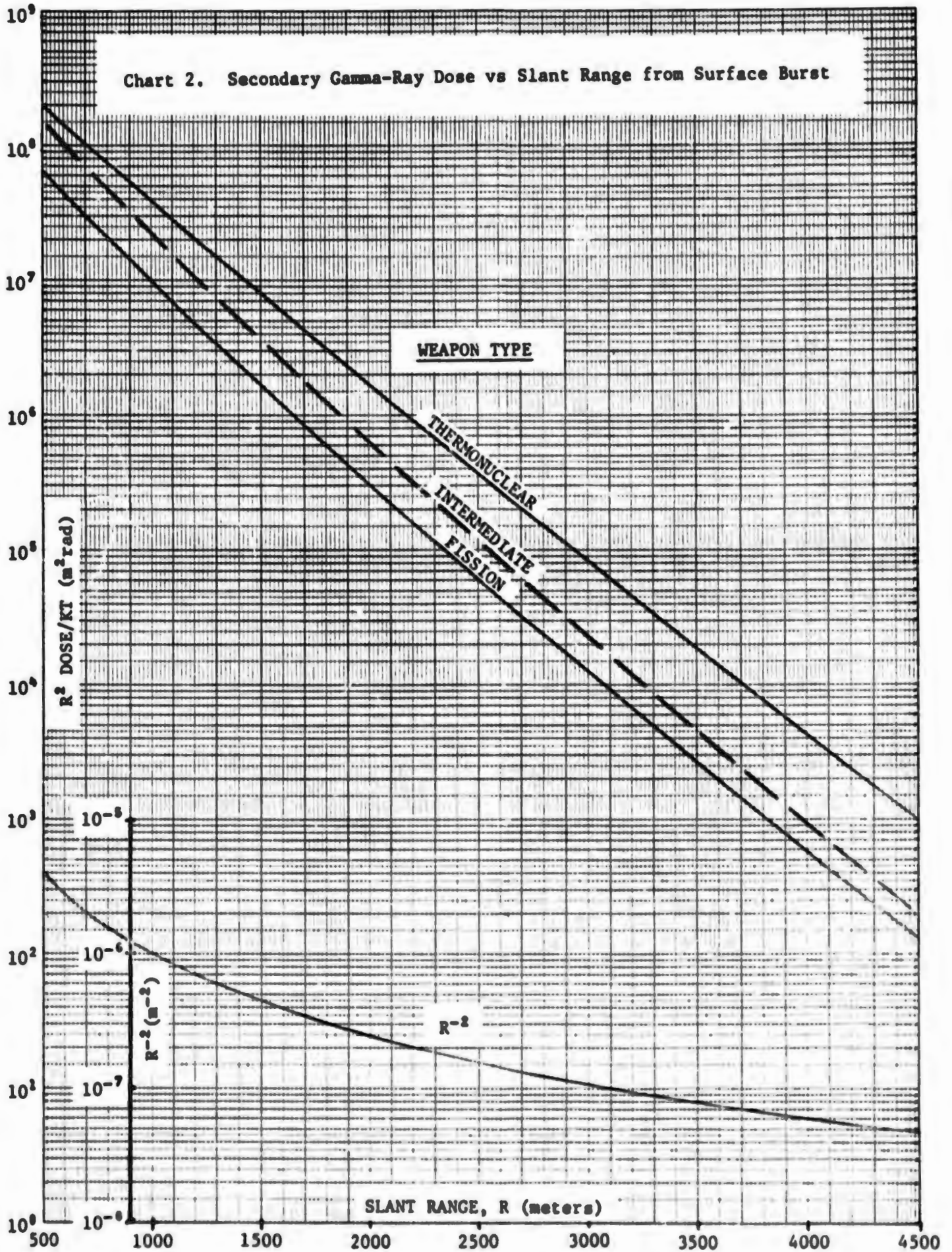


Chart 2. Secondary Gamma-Ray Dose vs Slant Range from Surface Burst



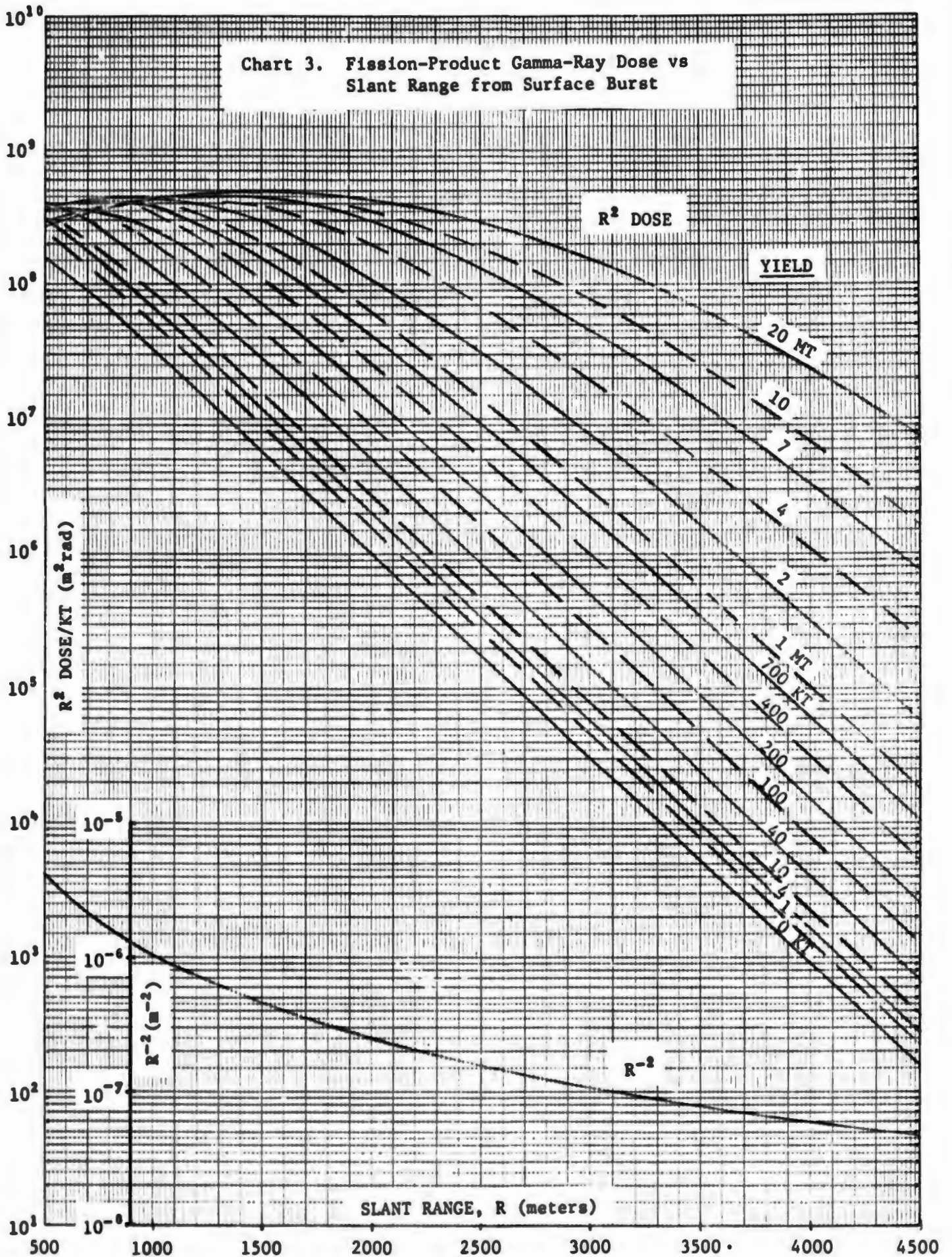


Chart 4. Scaled Slant Ranges for Various Air Densities

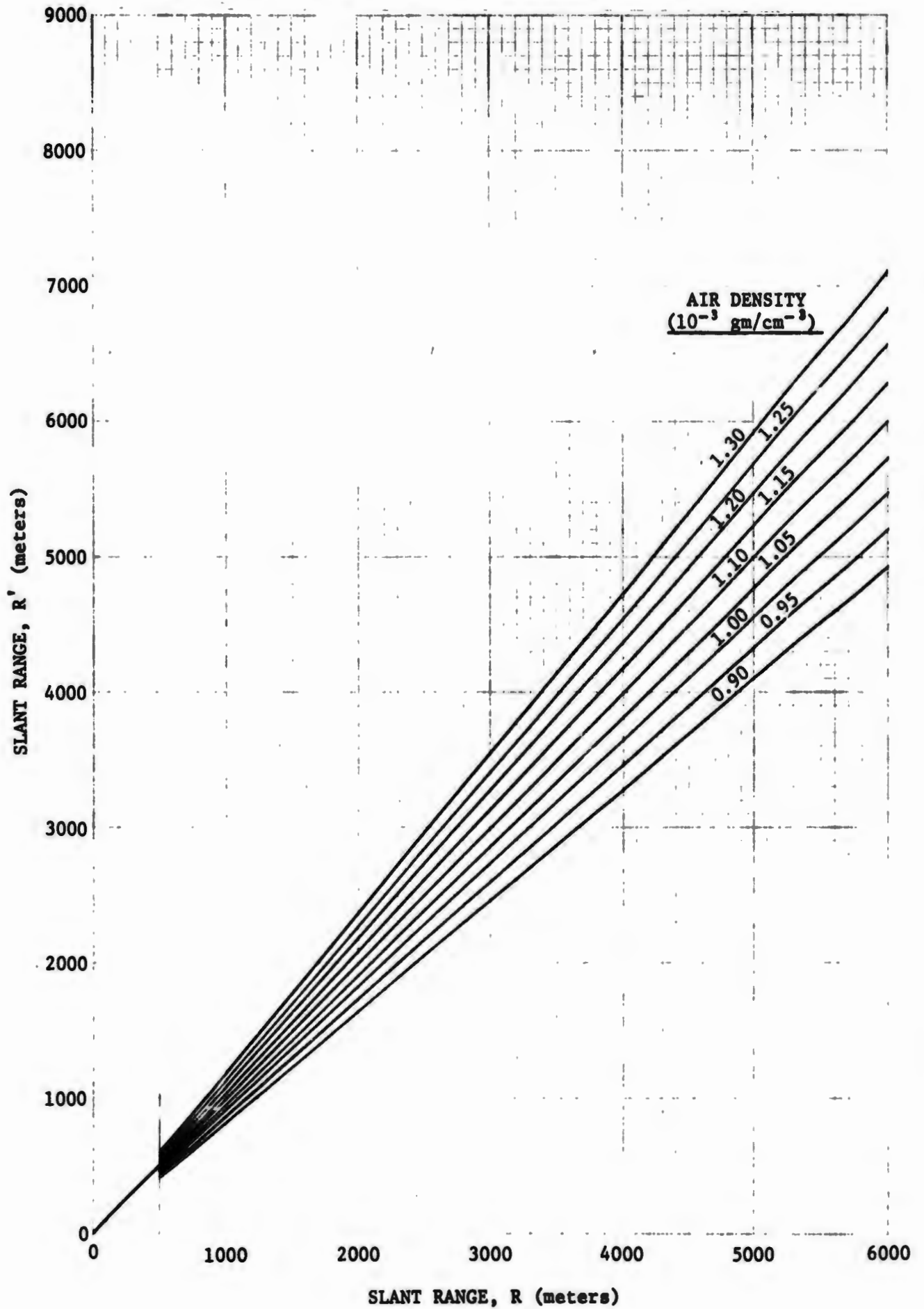


Chart 5. Burst Height Adjustment Factors for Neutrons and Secondary Gamma Rays

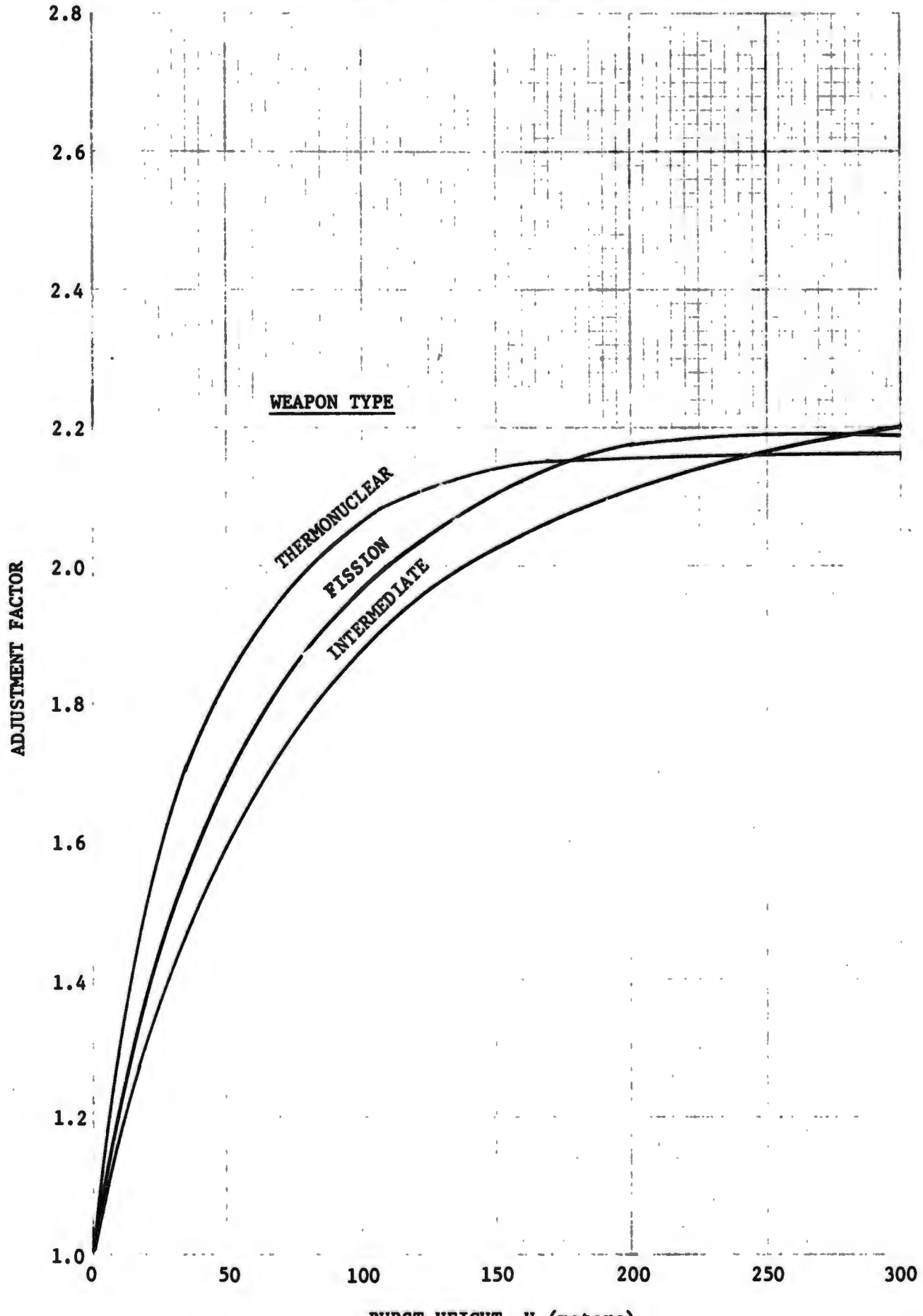
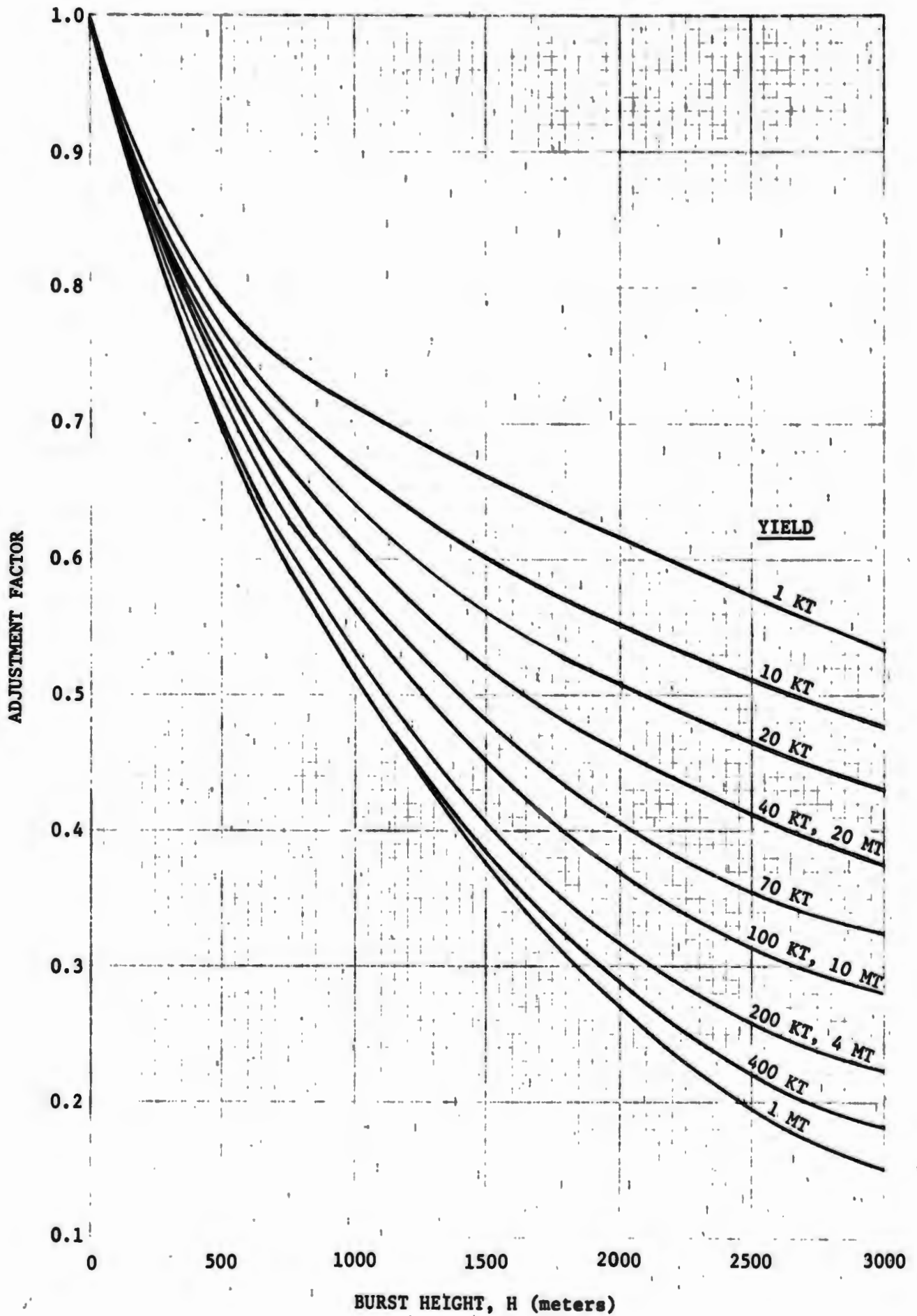


Chart 6. Burst Height Adjustment Factors
for Fission-Product Gamma Rays

VI. CONCLUSIONS

Improved methods were presented for predicting the initial neutron secondary gamma-ray and fission-product gamma-ray exposures following the detonation of a nuclear weapon. These methods incorporate the most appropriate radiation transport data, and the most effective techniques that could be found for treating the various phenomena involved.

Extensive comparisons with measured data and various calculated data were made to validate the methods. Comparison with the results of numerous weapon tests indicated that the neutron dose may be generally predicted within about 25% if the neutron leakage spectrum of the particular weapon is considered. The secondary-gamma method also appears to give reliable results. However, it is difficult to obtain direct experimental verification of this component because measured gamma-ray exposures from weapon tests are usually dominated by fission-product gamma rays.

A considerable portion of the study was devoted to a new method for predicting fission-product gamma-ray exposures. Fission-product gamma-ray exposures calculated with the new method, when combined with secondary gamma-ray exposures calculated with the above method, give results that generally agree with weapons test data within 25% for low-yield weapons and 50% for high-yield weapons.

To facilitate routine predictions of initial radiation exposures without performing detailed machine calculations, a highly simplified model was derived from the results of extensive parametric calculations performed with the detailed methods. This model gives fission-product gamma-ray results that agree with the detailed calculations within 20% in most cases and within 45% in all cases. The accuracy of the model for neutron and secondary gamma-ray results depends upon how well the weapon of interest is represented by one of three typical weapons included in the model.

REFERENCES

1. E. A. Straker, "Time-Dependent Neutron and Secondary Gamma-Ray Transport in an Air-Over-Ground Geometry," ORNL-4289, Vol. II, Oak Ridge National Laboratory (1968).
2. E. A. Straker and M. L. Gritzner, "Neutron and Secondary Gamma-Ray Transport in Infinite Homogeneous Air," ORNL-4464 (December 1969).
3. R. L. French, "A First-Last Collision Model of the Air/Ground Interface Effects on Fast-Neutron Distributions," Nucl. Sci. Engr. 19, 151-157 (1964).
4. E. A. Straker, "The Effect of the Ground on the Steady-State and Time-Dependent Transport of Neutrons and Secondary Gamma-Rays in the Atmosphere," Nucl. Sci. Engr. 46, 334-335 (1971).
5. L. G. Mooney and R. L. French, "A New Look at the Fission-Product Gamma-Ray Component of Nuclear Weapon Initial Radiation," ORNL-RSIC-33, Proceedings of the Radiation Transport in Air Seminar-Workshop (to be published).
6. R. L. French and L. G. Mooney, "Prediction of Nuclear Weapon Neutron-Radiation Environments," Nuclear Technology 10, 348-365 (1971).
7. Samuel Glasstone, editor, "The Effects of Nuclear Weapons," U. S. Atomic Energy Commission (1962).
8. V. I. Kukhtevich, et al, "Protection from Penetrating Radiation of a Nuclear Explosion," Atomizdat Press, Moscow (1970).
9. J. A. Auxier, Z. G. Burson, R. L. French, F. F. Haywood, L. G. Mooney, and E. A. Straker, "Nuclear Weapons Free-Field Environment Recommended for Initial Radiation Shielding Calculations," ORNL-TM-3396, Oak Ridge National Laboratory (1971).
10. L. B. Engle and P. C. Fisher, "Energy and Time Dependence of Delayed Gammas from Fission," LAMS-2642, Los Alamos Scientific Laboratory (1962). (See also Phys. Rev., 134 No. 4B, B796 - B816 (May 25, 1964).
11. F. R. Mynatt, "A User's Manual for DOT," USAEC Report K-1694, Oak Ridge Gaseous Diffusion Plant (to be published).
12. F. F. Haywood, "Spatial Dose Distribution in Air-Over-Ground Geometry," Health Physics 11, 185-192 (1965).

13. J. D. Marshall and M. B. Wells, "The Effects of Cut-Off Energy on Monte Carlo Calculated Gamma Ray Dose Rates in Air," RRA-M67, Radiation Research Associates, Inc. (1966).
14. F. F. Haywood, J. A. Auxier and E. T. Loy, "An Experimental Investigation of the Spatial Distribution of Dose in an Air-Over-Ground Geometry," CEX-62.14, U. S. Atomic Energy Commission (1964).
15. A. E. Fritzsche, N. E. Lorimier and Z. G. Burson, "Measured Low-Altitude Neutron and Gamma Dose Distributions Due to a 14-MeV Neutron Source," EGG 1183-1449, EG&G, Inc. (1969).
16. A. E. Fritzsche, N. E. Lorimier and Z. G. Burson, "Measured High-Altitude Neutron and Gamma Dose Distributions Due to a 14-MeV Neutron Source," EGG 1183-1438, EG&G, Inc. (1969).
17. Henderson, B. J., "Conversion of Neutron and Gamma Ray Flux to Absorbed Dose Rate", XDC 59-8-179 (1959).

APPENDIX

**Comparison of Initial Radiation Exposures Produced by Two
Different "Representative" Thermonuclear Weapons**

A "typical" intermediate yield thermonuclear weapon neutron leakage spectrum was suggested in ORNL-TM-3396.9 for use in initial radiation shielding calculations. A similar thermonuclear weapon neutron leakage spectrum has been selected* for use in the forthcoming new edition of Glasstone's, "The Effects of Nuclear Weapons."⁷ In view of the confusion that may arise from the use of similar but not quite identical typical thermonuclear weapons in the unclassified literature, and the wide distribution anticipated for the latter publication, the latter neutron leakage spectrum was selected for incorporation in the simplified model.

The similarity of the two weapons is illustrated by the following neutron and secondary gamma-ray dose ratios. These ratios were obtained by dividing doses calculated for the indicated ranges using the ORNL-TM-3396 spectrum by corresponding doses calculated using the Glasstone spectrum. The fission-product gamma-ray doses from the two devices are identical providing the same fission fraction is assumed for each.

<u>Range</u>	<u>Neutron Ratio</u>	<u>Secondary Gamma Ratio</u>
500	1.38	1.22
1000	1.39	1.24
1500	1.37	1.22
2000	1.35	1.20
3000	1.30	1.18
4000	1.24	1.17
5000	1.19	1.16

* P. Dolan, Stanford Research Institute, private communication (1972).